Coordinated cerebellar climbing fiber activity signals learned sensorimotor predictions

William Heffley II[1], Eun Young Song[1], Ziye Xu[1], Benjamin N. Taylor[1], Mary Anne Hughes[1], Andrew McKinney[1,2] , Mati Joshua[1,3] and Court Hull[1*]

[1]*Department of Neurobiology, Duke University Medical School, Durham, United States*

[2]*Present Address: Neuroscience Graduate Program, Baylor College of Medicine, Houston, United States*

[3]*Present Address: Edmond and Lily Safra Center for Brain Sciences, the Hebrew University, Jerusalem, Israel*

*Correspondence: Court Hull

Email: Hull@neuro.duke.edu

Abstract

The prevailing model of cerebellar learning states that climbing fibers (CFs) are both driven by, and serve to correct, erroneous motor output. However, this model is grounded largely in studies of behaviors that utilize hardwired neural pathways to link sensory input to motor output. To test whether this model applies to more flexible learning regimes that require arbitrary sensorimotor associations, we have developed a cerebellar-dependent motor learning paradigm compatible with both mesoscale and single dendrite resolution calcium imaging in mice. Here, we find that CFs are preferentially driven by and more time-locked to correctly executed movements and other task parameters that predict reward outcome, exhibiting widespread correlated activity within parasagittal processing zones that is governed by these predictions. Together, such CF activity patterns are well-suited to drive learning by providing predictive instructional input consistent with an unsigned reinforcement learning signal that does not rely exclusively on motor errors.

Introduction

A key role of the cerebellum is to form predictive associations between sensory inputs and motor outputs. These sensorimotor predictions are critical for generating well-timed and accurate movements, and in the absence of cerebellar function, the lack of such predictive motor output severely impairs our ability to generate coordinated responses to stimuli in the external world.

Classic models posit that the cerebellum generates sensorimotor predictions according to a supervised learning rule[1-3]. According to such models, projections from the inferior olive called climbing fibers are thought to signal motor errors, thus providing information to Purkinje cells about discrepancies between the expected consequences of a motor command and subsequent sensory feedback. To correct erroneous motor output, climbing fibers instruct heterosynaptic long-term depression[4,5] by producing powerful regenerative calcium transients[6] in Purkinje cell dendrites called complex spikes[7]. In so doing, climbing fibers are thought to appropriately update the cerebellar forward internal model with revised sensorimotor predictions.

This supervised error-signaling framework provides a compelling explanation for climbing fiber activity in a variety of simple behaviors, such as classical conditioning (e.g. eyeblink conditioning) and adaptation (e.g. vestibulo-ocular reflex gain changes)[8-10] paradigms. Such behaviors typically rely on a yoked relationship between unconditioned sensory input and

motor output, allowing the cerebellum to utilize signals from hardwired pathways to drive learning. Hence, the climbing fibers can instruct learning by responding to an unconditioned stimulus (e.g. periocular eye puff or retinal slip) that produces the same movement requiring modification (e.g. eyelid closure or eye movement).

However, many forms of motor learning do not involve modifications to motor programs linked directly to an unconditioned stimulus and response. Instead, the correct association between sensory input and motor output must be learned through experience, and the sensory information necessary for learning may have no direct relationship to the movement that requires modification. Such abstract associations necessitate that learning cannot be achieved by input from hardwired pathways alone. In these cases, where an unconditioned stimulus and response alone do not contain sufficient information to guide learning, it is unclear how a supervised error signal could be generated, or whether such a learning rule could account for either climbing fiber activity or the cerebellar contribution to learning.

To test how the climbing fiber system is engaged under conditions where the sensory and motor signals necessary to drive learning are not innate, we have established a cerebellar-dependent behavioral paradigm compatible with population level *in vivo* calcium imaging, optogenetic and electrophysiological approaches. Using this paradigm, we reveal two key features of climbing fiber (CF) driven complex spiking. First, we find that complex spiking cannot be accounted for by a simple error-based supervised learning model. Instead, complex spiking can signal learned, task specific predictions about the likely outcome of movement in a manner consistent with a reinforcement learning signal. Second, population level recordings reveal that while complex spiking is correlated within parasagittal zones, these correlations also depend on behavioral context. While previous measurements have shown increased correlations in complex spiking in response to sensory input or motor output[11-14], and have suggested an important role for synchrony in downstream processing and motor learning[15], our results reveal that such modulation can vary for identical movements depending on behavioral relevance. Hence, these data reveal key features of cerebellar CF activity that differ significantly from many classically studied cerebellar behaviors, and suggest an extension to current models of cerebellar learning in order to account for the role of complex spiking in tasks that require abstract sensorimotor associations.

Results:

To measure climbing fiber driven complex spiking, we first designed an appropriate task. An important feature of the task design is to specifically engage neurons near the dorsal surface

104 of the cerebellum, thereby allowing for visualization of complex spikes via calcium imaging.
105 Hence, we used optogenetics to functionally map the midlateral dorsal surface of the mouse
106 cerebellum according to the motor output produced by spatially defined populations of Purkinje
107 cells (PCs). To do so, we expressed Archaerhodopsin (Arch) using a transgenic approach
108 (methods) in cerebellar PCs (Fig. 1A), and used an external fiber coupled laser to transiently
109 suppress PCs near the dorsal surface of the cerebellum (Fig. 1B). Consistent with previous
110 work[16], we identified a population of superficial PCs in lobule simplex capable of driving
111 ipsilateral forelimb movements either during optogenetic silencing or following a brief train of
112 electrical simulation (Fig. 1, Supp. Fig. 1, Supp. Video 1). *In vivo* single unit recordings
113 confirmed that our optogenetic stimulation was effective in silencing superficial PCs at the
114 threshold for driving forelimb movement (~20 mW) up to a depth of 500 μm (Fig. 1B).
115
116 **A cerebellar dependent sensorimotor association learning task**
117 We next designed a sensorimotor association task involving forelimb movement, with the
118 rationale that the cerebellar contribution to learning in such a task should necessarily involve the
119 PCs capable of driving forelimb movements. This task contains two discrete conditions; one
120 where motor output is reactive ('cue reaction'), and another where motor output becomes
121 predictive with learning ('cue prediction'). In both task variations, head restrained, water
122 deprived mice are trained to self-initiate trials by depressing a lever, and to release the lever in
123 response to a visual cue (Fig. 1C,D).
124 In the cue reaction condition, trial-to-trial variability in the timing of the visual cue (Fig.
125 1E,G, Supp. Video 2) is imposed to necessitate that mice employ reactive forelimb responses.
126 In this regime, reaction times are reflective of the latency for sensory integration[17] and remain
127 constant throughout each session (Fig. 1H).
128 In the cue prediction condition, by presenting the visual cue with a constant delay on
129 every trial, mice learn to predict the timing of the cue and adjust their motor responses to more
130 closely approximate its timing (Fig. 1F,G). Moreover, learning occurs within single training
131 sessions, is retained across days (Supp. Fig. 2A), and can be extinguished by returning mice to
132 the cue reaction paradigm (Supp. Fig. 2C,D). In addition, we find that learning depends on the
133 duration of the cue delay: maximal learning occurs at short cue delays (e.g. 500 ms) and little or
134 no learning occurs for cue delays greater than 1.5 seconds (Fig. 1H; one-way ANOVA, main
135 effect of cue delay, $p = 4.8 \times 10^{-6}$. Post hoc comparison to cue reaction: 500 ms, $p=1.9 \times 10^{-11}$, 1 s,
136 $p=8.4 \times 10^{-11}$, 1.5 s, p=0.359, 2 s, p=0.005). This dependence on a short interval delay is
137 consistent with the temporal characteristics of canonical cerebellar-dependent sensorimotor

138 associative learning[18].

139 To test whether animals adjust the timing or kinematics of forelimb movement to predict
140 the visual cue, we measured lever kinematics during a subset of learning sessions. Alignment
141 of the lever trajectory to the cue onset confirmed that animals released the lever sooner in
142 anticipation of the visual cue (Fig. 1I; $p = 1.2x10^{-5}$, paired t-test). However, despite substantial
143 variability in the kinematics of release (Supp. Fig. 3), independent alignment of both press and
144 release demonstrated that there was no change in movement kinematics across learning
145 sessions (Fig 1I-J; p=0.513, paired t-test).

146 To test the necessity of lobule simplex for this learning, we first locally applied lidocaine
147 to block spiking in cerebellar cortical neurons, including PCs. However, consistent with the
148 critical tonic inhibition PCs provide to the deep cerebellar nuclei, we observed significant motor
149 deficits including slowed movement, dramatically fewer initiated trials, and dystonic limb
150 contractions (not shown). Thus, this manipulation was not appropriate to define the necessity of
151 lobule simplex in our task.

152 To avoid significant motor impairment, we next used a pharmacological manipulation to
153 selectively disrupt excitatory synaptic transmission in lobule simplex without abolishing PC
154 pacemaking. For these experiments, we optimized concentrations of the excitatory synaptic
155 transmission blockers NBQX (300 μM), CPP (30 μM) and MCPG (30 μM) to avoid visible
156 impairment of motor output, and then tested this cocktail during behavior. Following local drug
157 application (methods), mice retained the ability to release the lever in response to the visual
158 cue, maintaining stable kinematics across sessions (Fig. 2A,B) that were not different from
159 control sessions (Fig. 1I,J, and Supp. Fig. 3; Press p=0.261; Release p=0.222, unpaired t-test).
160 However, despite stable movement kinematics, learning was severely impaired when the cue
161 was presented with a constant 500 ms delay (Fig 2A,C,D) (NBQX vs Control 500 ms $p=4.6x10^{-}$
162 ^{4}, NBQX vs Control Cue Reaction p=0.05, unpaired t-test). Acute single unit PC recordings
163 during drug application revealed that this manipulation significantly reduced complex spike
164 rates, consistent with a reduction in the amplitude of postsynaptic glutamatergic currents
165 produced by climbing fiber input (Supp. Fig. 4; $p=8.5x10^{-4}$, paired t-test). We also found a trend
166 toward decreased simple spiking, consistent with reducing synaptic input from the mossy fibers
167 and parallel fibers (p=0.36, paired t-test). Hence, these data support that hypothesis that
168 synaptic transmission in lobule simplex is necessary for predictive sensorimotor learning in our
169 task, thus implicating cerebellar cortical learning.

170

171 **Complex spiking is not driven by motor errors in a voluntary motor learning task**

172 Because climbing fibers provide key instructional signals for cerebellar learning, we next
173 sought to test what information is conveyed by the olivary system in this behavior. Thus, we
174 imaged climbing fiber evoked calcium signals in mice engaged in the cue reaction condition. In
175 this regime, all sensorimotor signals are in place to drive learned, predictively timed forelimb
176 movements, but no learning can occur due to the variable cue timing (Fig. 1G,H). Hence, we
177 can test what task features drive complex spiking in a stable regime. We began by using a
178 single photon microscope to image populations of PCs virally expressing GCaMP6f (methods).
179 Image segmentation in a subset of experiments with the most superficial GCaMP expression
180 revealed structures consistent in size and shape with PC dendrites in cross section, and these
181 structures exhibited calcium transients at rates consistent with the baseline rate of complex
182 spiking measured with single unit electrophysiology (Supp. Fig. 5). These results are consistent
183 with several *in vivo* calcium imaging studies showing that PC responses are dominated by the
184 large dendritic calcium transients produced by complex spikes[11-14, 19-24].
185 We next identified regions of interest, defined by the expression pattern of GCaMP in
186 each animal, that were restricted to the region within lobule simplex capable of driving ipsilateral
187 forelimb movements (methods). Consistent with the role of this region in the control of forelimb
188 movements, we observed task modulated PC calcium transients associated with the timing of
189 lever press and release, with the largest modulation at the time of lever release (Fig. 3A-C).
190 Surprisingly, when we segregated trials according to outcome, we observed significantly larger
191 calcium transients at the time of lever releases when animals correctly released the lever in
192 response to the visual cue (Fig. 3A-D; $p=4.60\times10^{-5}$, paired t-test). These enhanced responses
193 were distributed widely across dorsal, superficial lobule simplex, and were consistent across
194 sessions and animals. The same pattern of enhanced complex spiking on correctly timed lever
195 releases was observed in the cue prediction condition, and was maintained across learning
196 sessions, as measured by single unit PC electrophysiological recordings (Supp. Fig. 6). Thus, in
197 this task, our data suggest that complex spikes occur preferentially on correctly timed
198 movements, and not following motor errors.
199 There are many differences between correct and early release trials that could contribute
200 to the outcome-dependent difference in complex spiking. One possible difference between trial
201 types could be the kinematics of forelimb movement. Hence, in a subset of our experiments, we
202 measured movement kinematics by comparing lever trajectories on correct and early release
203 trials (Fig. 4A-B). These data revealed closely matched movement kinematics between correct
204 and early lever release trials (Press $p = 0.06$, Release $p = 0.007$, paired t-test).

205 Another difference between correctly timed and early lever releases is that reward is
206 only delivered on correct trials, and this results in extended licking. Indeed, we find that lick
207 rates were significantly higher on correct trials (Fig. 4C; $p=3.74x10^{-9}$, paired t-test). Moreover, in
208 some sessions we observed a late, sustained calcium transient that occurred during licking (Fig.
209 4D). However, we found no correlation between the mean peak calcium transients and mean
210 lick rates across trial types (Fig. 4E,F; Correct p=0.11; Early p=0.98, linear regression) or within
211 sessions across trials of each type (Fig. 4G; Correct p=0.93; Early p=0.65, one sample t-test;
212 Supp. Fig. 7D; Correct p=0.544; Early p=0.428, one sample t-test). Thus, we conclude that the
213 enhanced responses as measured by the peak calcium transient on correctly timed lever
214 releases are not due to differences in forelimb movement kinematics or licking (Fig. 4 and Supp.
215 Fig. 7), but are instead linked to the context of the movement.
216
217 **Behavioral context determines the probability and synchrony of complex spiking**
218 To investigate the dynamics of complex spiking at the single cell level, we used video-
219 rate two-photon microscopy to image the dendrites of PCs during behavior. Using this
220 approach, we isolated the dendrites of individual PCs[20] (Fig. 5, Supp. Figs. 5, 8), and measured
221 both spontaneous and task-evoked calcium transients. As with the single photon imaging
222 experiments, spontaneous calcium transients measured during inter-trial intervals occurred at a
223 rate of 0.61 ± 0.01 Hz, consistent with our electrophysiological measurements of spontaneous
224 complex spiking (Supp. Fig. 5E,F). The two-photon data also replicated the main finding that the
225 mean calcium transients were significantly larger on correct release trials within individual PC
226 dendrites (Fig. 5A,B; $p=9.79^{-76}$, paired t-test). Moreover, lever releases that were rewarded but
227 occurred too fast to be responses to the visual cue (reaction times < 200 ms) produced calcium
228 transients that were significantly smaller than those produced by correct lever release trials
229 ($p=3.91^{-104}$, paired t-test) and not significantly different from responses on early release trials
230 (p=0.086). Hence, these data support the analysis in Figure 4 that the enhanced complex
231 spiking on correct trials is not due to licking or reward per se.
232 In addition to larger mean responses across trials, population level analysis revealed
233 that more PCs were driven on correct release trials (Fig 5C). Of the total PC population that
234 responded to any lever press or release (1146 of 1302), most (88%) PCs exhibited complex
235 spikes on correct release trials, whereas less than half (41%) responded during early lever
236 releases (Fig. 5D, *top*). Approximately half (48%) exhibited complex spikes in response to lever
237 press (Fig. 5D, *bottom*). The increased number of active dendrites on correct trials is unlikely to
238 be a thresholding artifact, since there was no significant difference in the average response

239 amplitude of correct-only and correct+early responsive dendrites to correct trials (p=0.44,
240 unpaired t-test, correct-only n=578 dendrites, correct+early n=457 dendrites). These data also
241 indicate that the measured increase in number of active dendrites is not due to contamination of
242 fluorescent signals from neighboring dendrites. Hence, these single dendrite measurements
243 explain our single photon results by demonstrating that both more PCs exhibit complex spikes
244 on correct trials, and those dendrites that exhibit complex spikes in response to both trial types
245 have larger mean calcium transients on correct trials.

246 The difference in the average release-evoked response on correct versus early trials
247 may be due to a difference in the amplitude of the calcium transients on each trial. For instance,
248 complex spikes are not "all-or-none" events[25], and the number of spikelets can vary from event
249 to event[26], altering the size of the evoked calcium transient[27]. Thus, we extracted single trial
250 events associated with lever releases across trial types, and compared these with each other
251 and to spontaneous calcium transients. However, this analysis revealed no significant difference
252 between the amplitude of calcium transients on single trials in response to either correct or early
253 lever releases, and between movement-evoked and spontaneous activity (Fig. 5E; p=0.17, one-
254 way ANOVA). Thus, if there are variable numbers of evoked spikelets across trials, such
255 differences are not systematically correlated with either trial outcome or task engagement.
256 Moreover, the equivalent amplitude of lever-evoked and spontaneous events suggests that the
257 majority of the signal measured in response to lever release is due to complex spiking. Indeed,
258 the size and shape of our segmented ROIs is consistent with several studies showing that
259 complex spikes produce a calcium signal throughout the entire PC dendrite[28, 29], whereas
260 parallel fiber calcium signals are much smaller and confined to isolated regions of spiny
261 dendritic branchlets[30, 31].

262 To assess how equivalent single event responses can produce larger mean responses
263 on correct trials, we generated a peristimulus time histogram of complex spike events for each
264 trial type aligned to the time of release (Fig. 6A). This analysis revealed a significantly
265 enhanced complex spike rate at the time of lever release when movement was correctly timed
266 (Fig. 6A,B; $p=8.14\times10^{-15}$, paired t-test). In addition, complex spiking on correct trials in single
267 PC dendrites occurred with shorter latency (Fig 6C; $p=2.65\times10^{-11}$, paired t-test) and less
268 temporal jitter across trials (Fig 6D; p=0.007, paired t-test). Notably, these measures of jitter are
269 likely to be an overestimate, since our measure of event time is limited by our sampling interval
270 (33 ms). However, when accounting for the overall spontaneous event rate of ~1 Hz, the 100
271 ms jitter of events on correct trials is comparatively precise.

The PSTH reveals that elevated complex spiking occurs proximal to lever release. To test whether the increase in complex spiking is more closely associated with the lever release or the visual cue, we compared the temporal jitter of spike times on correct trials when aligned to each of these events. This analysis revealed a significantly lower temporal jitter when the spikes were aligned to lever release as measured either with imaging (Fig 6F; $p=6.2x10^{-5}$, paired t-test) or at higher temporal resolution with electrophysiology (Supp. Fig. 6F; $p=7.8x10^{-9}$; paired t-test). Notably, the closer association between spiking and the lever release was maintained across learning in cue prediction sessions, even as lever releases moved closer to the timing of the visual cue (Supp. Fig. 6E-F). In addition, we find that the latency to peak event rate is strongly correlated with reaction time when the events are aligned to visual cue (Fig 6G; $p=8.56x10^{-12}$, Pearson's correlation), but not when aligned to lever release ($p=0.13$). These results further suggest a closer association between lever release and complex spiking than for the visual cue and complex spiking.

The narrower PSTH on correct release trials is also consistent with the possibility of enhanced synchrony on the time scale of ~100 milliseconds at the population level. Indeed, we find enhanced population synchrony across dendrites (Fig 6E; $p=0.003$, paired t-test). However, in many experiments, we observed no such increase in population synchrony on correct trials (16 out of 30 sessions do not have significantly elevated synchrony on correct trials, open circles, $p>0.05$ for each session). We thus considered the possibility that enhanced synchrony was location specific, and might obey spatial structure that was not well demarcated at the scale of the field of view in our two-photon experiments.

Context determines correlated population activity at the mesoscale level

To investigate whether correlated complex spiking was spatially organized, we used an unsupervised, iterative pixel-clustering approach[22] (methods) to assess correlations between pixels across all trials at the mesoscale level from single photon imaging sessions with widespread GCaMP expression (Fig. 7A). Despite non-uniform, unpatterned GCaMP expression, this analysis revealed spatial patterns of correlated activity that were organized across parasagittal bands oriented in the rostro-caudal axis. These bands were 221 ± 15 μm wide on average across 39 measured zones, consistent with previous anatomical and physiological measurements of cerebellar microzones[32]. Hence, these data support the longstanding hypothesis that the anatomical pattern of climbing fiber projections into the cerebellar cortex establishes functionally distinct parasagittal processing modules.

305 To test how complex spiking is modulated during behavior within and across parasagittal
306 zones, we divided trials according to outcome and analyzed brief epochs surrounding the time
307 of lever release (Fig. 7B). While this analysis lacks the fine temporal resolution of the two-
308 photon event based analysis in Figure 6, it nonetheless revealed that activity amongst pixels
309 within a zone exhibited higher correlations for most zones on correct lever release trials (Fig.
310 7C; $p = 1.60 \times 10^{-5}$, paired t-test). These enhanced correlations are not an artifact of elevated
311 complex spike rates on correct trials because early release trials still had weaker correlations
312 across equivalent activity levels as assessed by linear fits to bootstrapped distributions paired
313 from each trial type (methods) (Fig. 7D). We also found enhanced correlations between
314 neighboring and non-neighboring zones on correct lever release trials (Fig. 7E,F; Neighboring
315 $p=0.004$, Non-Neighboring $p=6.2 \times 10^{-12}$, paired t-test). However, these cross-zone correlations
316 were significantly lower on average than those within zones (Within Zone vs Neighboring,
317 $p=0.004$; Within Zone vs. Non-Neighboring $p=3.4 \times 10^{-4}$, unpaired t-test). Hence, these data
318 reveal a precise spatial organization of climbing fiber activity, with highly correlated complex
319 spiking within parasagittal zones that is task specific, differing for movements with the same
320 kinematics depending on behavioral context.
321
322 **Complex spiking signals learned sensorimotor predictions**
323 Our data suggest that complex spiking does not signal motor errors in this behavioral
324 paradigm. Instead, our results are consistent with the possibility that the climbing fibers either 1)
325 instruct a different type of supervised learning rule based on correctly timed motor output, or 2)
326 provide a reinforcement learning signal, such as a temporal-difference (TD) signal of the type
327 recently identified for climbing fibers during conditioned eyeblink learning[33]. While the
328 instructional signals for supervised learning encode specific outcomes, those for reinforcement
329 learning are driven by prediction errors. Thus, while a reinforcement learning signal should
330 occur to any unexpected outcome (e.g. unexpected reward) or event that predicts task outcome,
331 a supervised signal based on correct movements should only occur for correctly timed arm
332 movements. We hence began by testing whether climbing fibers can be driven by unexpected
333 reward.
334 Surprisingly, when reward was delivered unexpectedly during the intertrial interval, we
335 observed robust climbing fiber responses of similar amplitude to those driven by correctly timed
336 lever releases (Figure 8A, Supp. Fig. 9). Because we have already demonstrated that the
337 increase in climbing fiber activity is not driven by licking or reward (Figs. 4, 5B, Supp. Figs. 7,9),
338 we interpret the increase in complex spiking in response to an unexpected reward as evidence

339 of a prediction error. We hence conclude that climbing fibers do not specifically represent
340 correctly timed movement per se, but may instead provide input consistent with a reinforcement
341 learning rule.

342 To further test whether climbing fiber activity in our task is consistent with a
343 reinforcement learning signal, we next tested whether the climbing fibers respond to other task
344 features that predict task outcome (reward delivery). Thus, we took advantage of the temporal
345 structure of the task, wherein the probability of cue appearance, and thus reward delivery,
346 increases with lever hold time (i.e. the hazard function is not flat). We specifically tested
347 whether complex spiking depends on lever hold time for correct and early lever releases.

348 We find that while complex spiking is independent of lever hold time for correctly timed
349 movements (Fig. 8B; 2-photon $p=0.98$, Supp. Fig.10; 1-photon $p=0.76$, Spearman's
350 correlation), there is a strong positive relationship between hold time and complex spiking for
351 early releases across both single and multiphoton imaging sessions (2-photon $p=4.58\times10^{-6}$, 1-
352 photon $p<1.0\times10^{-16}$, Spearman's correlation). The elevated complex spiking associated with
353 longer hold times (Fig. 8C) is due to both an increase in spiking at the time of release (Fig. 8E;
354 Window 1 $p=3.84\times10^{-10}$, paired t-test), and an additional late response not present on short
355 duration early release trials (Fig. 8F; Window 2 $p=1.33\times10^{-25}$; paired t-test). The late response
356 occurred on single trials and within individual dendrites, indicating that it was not generated by a
357 diversity of response timings across trials or by a separate population of PC dendrites (Fig. 8D).
358 In addition, the late response occurred approximately 200 ms after lever release when reward
359 was no longer possible and lick rates began to decrease (Fig 8 H,I). This provides additional
360 evidence that increases in licking cannot explain the observed increases in complex spiking.
361 Instead, this result reveals that licking is tightly linked to the animals' expectation: when the
362 animal no longer expects reward, lick rates decrease. In the same manner, because
363 spontaneous licks can reflect an expectation of possible reward, it is not surprising that
364 spontaneous licks are sometimes associated with increases in complex spiking (Supp. Fig. 7).

365 Each of these results are consistent with a reinforcement learning rule based on
366 prediction error, where complex spiking increases in response to learned task events that
367 predict reward and unexpected outcomes (i.e., the lack of reward following long duration early
368 releases). In this model, an initial prediction accompanies lever release that depends primarily
369 on cue presentation. Thus, complex spiking in response to correct releases is significantly
370 stronger than on early releases, even for long duration holds (Fig. 8G; Window 1 $p = 3.16\times10^{-7}$,
371 paired t-test). However, while the visually driven lever release provides the strongest prediction
372 of trial outcome, trial duration also contributes to expectation according to the task structure. In

373 the case that initial expectation is unmet, the climbing fibers also signal this unexpected
374 outcome through an increase in spiking. Notably, this latter result argues that climbing fibers
375 encode an unsigned prediction error, in which there is an increase in spiking regardless of the
376 direction of the prediction error.

377 To further test this model, we performed another set of experiments to probe the role of
378 violated expectations in driving complex spiking. In these experiments, we omitted reward
379 delivery on 20% of correctly timed lever releases (Fig. 8 J-N). Consistent with the cue
380 appearance establishing expectation at the time of lever release, both rewarded and omission
381 trials resulted in calcium transients that were nearly equivalent at the time of lever release (Fig.
382 8L; Window 1 $p=0.04$, paired t-test). However, omission trials resulted in an additional, late
383 response at the time when reward delivery was no longer possible and lick rates began to
384 decrease (Fig. 8M; Window 2 $p=2.54\times10^{-9}$, paired t-test). The timing of this late response was
385 similar to the late response following long duration early releases, and was present on single
386 trials and within individual dendrites (Figure 8J,N). Hence, these experiments support the
387 hypothesis that climbing fibers can both signal and evaluate predictions about the likely
388 outcome of movements in a manner consistent with a reinforcement learning rule.
389

390 **Discussion**

391 We have established a sensorimotor association task that involves PCs near the dorsal
392 surface of lobule simplex. This behavior has several hallmarks of cerebellar learning, including
393 a dependence on short delay intervals for generating the learned sensorimotor association and
394 the requirement for excitatory synaptic transmission in the cerebellar cortex. In this behavior,
395 however, climbing fibers do not signal erroneous motor output as described by classical models
396 of supervised learning. Specifically, we demonstrate that climbing fiber driven complex spiking
397 occurs with higher probability, shorter latency, and less jitter when movement is correctly timed.

398 Our data support the hypothesis that these enhanced climbing fiber responses are
399 related to the predicted outcome of movement, which in this behavior constitutes delivery of a
400 water reward. Evidence supporting this model is threefold: First, the highest probability of
401 complex spiking occurs on correctly timed lever releases when the visual cue instructs behavior
402 and thus a high reward expectation. Second, complex spiking is modulated by the temporal
403 features of the task that dictate expectation. Specifically, complex spiking in response to lever
404 release increases with increasing hold duration, matching the increased likelihood of reward as
405 trial length increases. Third, complex spiking is also driven when the expectation of reward is
406 violated: when the reward is omitted on correctly executed movements, not provided on longer

407 hold duration early releases when a correct outcome of lever release is probable, or
408 unexpectedly presented during the inter-trial interval. Together, these experiments suggest that
409 climbing fibers carry instructional signals that both predict and evaluate the expected outcome
410 of movement in a manner consistent with a reinforcement learning rule. Such responses are
411 also consistent with the known role of cerebellar circuits in generating predictive motor output,
412 and we suggest that they could thus provide a substrate for generating and testing the type
413 forward models that have long been hypothesized to govern cerebellar processing.

414 The climbing fiber activity observed in response to violated expectations has some
415 similarities to the motor error signals seen in classic cerebellar behaviors. However, in our
416 behavioral paradigm, climbing fibers do not signal movement errors, and correct movements
417 have the same kinematics as mistimed movements. Thus, these results indicate that climbing
418 fibers can respond differentially to the same movement according to its expected outcome.
419 These context-specific climbing fiber responses may be due to aspects of our task design. The
420 behavior described here differs from most cerebellar dependent learning regimes in that the
421 movement requiring modification (lever release) is not directly related to an unconditioned
422 stimulus (reward) or response (licking). As a consequence, the cerebellum cannot harness
423 sensorimotor input from hardwired pathways to enable learned changes in motor output.
424 Instead, the necessary forward model must define and evaluate the relationship between a
425 neutral visual stimulus, a forelimb movement, and reward.

426 It remains unclear whether the climbing fiber activity that enables such a forward model
427 is generated at the level of the olive or inherited from upstream brain regions such as the
428 neocortex, colliculus, or elsewhere. However, evidence suggests that the olive may have
429 access to different information depending on task requirements. Anatomical and physiological
430 work in the rodent has demonstrated that the pathway from the forelimb region of motor cortex
431 to the olive is independent of the pathway providing ascending sensorimotor input from the
432 periphery[34]. Such data argue that the olive has access to unique information in tasks that
433 involve a descending motor command, and further suggest that the olive may have access to
434 diverse cortical computations. Indeed, the presence of abstract task timing information
435 suggests that the olive has access to higher-order signals. In support of this view, evidence
436 from a different forelimb task in non-human primates that also requires an abstract sensorimotor
437 association has shown similar climbing fiber responses[35]. Specifically, this study demonstrated
438 that complex spikes can signal both the predicted destination of reaching as well as deviations
439 from the expected destination.

440 Importantly, the climbing fiber activity patterns described here are appropriate to drive
441 motor learning under conditions that require flexible sensorimotor associations. Specifically,
442 higher probability complex spiking and enhanced correlations at the population level are both
443 context dependent and spatio-temporally organized. At the population level, our single photon
444 imaging has revealed correlated complex spiking within parasagittal bands of approximately 200
445 μm, likely corresponding to "microzones"[32]. Because PCs across microzones can respond to
446 different sensorimotor input, and have different spiking[36] and synaptic[37] properties, these zones
447 are thought to constitute discrete computational units. Recent measurements have revealed that
448 complex spiking in microzones can become more synchronous during both motor output[14] and
449 sensory input[11, 12, 23]. Our population imaging results provide an extension to this idea by
450 demonstrating that correlated complex spiking within parasagittal zones is not simply enhanced
451 by sensorimotor input, but rather can be enhanced for the same action according to behavioral
452 context. Precisely timed spiking across a population of nearby PCs that receive common
453 parallel fiber input and converge to the same DCN neurons would provide an ideal substrate to
454 maximize the impact of plasticity. However, other circuits could also play a role in learning. In
455 particular, complex spiking can robustly inhibit nuclear neurons[38, 39], and enhanced climbing
456 fiber synchrony would magnify this effect via convergence of simultaneously active PC axons in
457 the DCN[40]. Because synchronous inhibition has been shown to play a key role in synaptic
458 plasticity at nuclear neuron synapses[41, 42], correlated complex spiking across populations of
459 nearby PCs could place the DCN as the central site of learning under such conditions[43]. In
460 either case, we note that the climbing fiber responses following correct lever releases are well-
461 timed to promote learning in the cue prediction condition by instructing movements that more
462 closely approximate earliest time of reward delivery.
463 Finally, it is notable that ours are not the first results to suggest alternate learning rules
464 instructed by climbing fibers. Recently, conditioned eyeblink learning data has pointed toward
465 climbing fibers implementing a temporal difference (TD) reinforcement learning rule by signaling
466 sensory prediction errors[33]. Because we do not observe evidence of negative prediction errors
467 on reward omission trials or long duration early release trials, our results are incompatible with
468 this model as strictly interpreted. Instead, our data show some similarities with the type of
469 unsigned prediction signals observed in serotonergic[44] and other neurons[45, 46] that have been
470 also thought to enable associations between unexpected outcomes and novel cues[47]. Evidence
471 for both models can often be found in neural activity within the same brain region, and it has
472 been suggested that TD and unsigned prediction mechanisms may in fact be linked, and act
473 together to promote learning[48]. Hence, as has been done in other brain regions, it will be

necessary to systematically vary task parameters such as the valence of instructional stimuli and the requirements for learned associations in order to resolve how the cerebellum implements discrete learning rules according to task demands beyond their classic role in supervised learning[49]. For the present, the results described here demonstrate that complex spiking can signal learned, task specific information necessary for flexible control of complex motor behaviors in a manner that does not depend exclusively on motor errors.

Data and Code Availability Statement

Data analysis code is available from the corresponding author upon reasonable request. The data that support the findings of this study are also available from the corresponding author upon reasonable request.

Acknowledgements:

This work was supported by grants from the NIH NINDS (5R01NS096289-02) (CH) and (F31NS103425) (WH), the Sloan Foundation (CH), and the Whitehall Foundation (CH). We thank L. Glickfeld for helpful discussions and input on calcium imaging approaches and analyses, S. Lisberger, G. Field, K. Franks and F. Wang for feedback on early versions of this manuscript, and members of the Hull and Glickfeld labs for input and technical assistance throughout the project.

Author Contributions

WH, ES, and CH designed experiments, WH, ES, AM, BT, MAH, and MJ conducted experiments, WH, ES, ZX, BT, AM, MJ, and CH analyzed data, and CH wrote the manuscript.

Competing Interests

The authors declare no competing interests.

References

1. Albus, J.S. A theory of cerebellar function. *Mathematical Biosciences* **10**, 25-61 (1971).
2. Ito, M. Neural design of the cerebellar motor control system. *Brain Res* **40**, 81-84 (1972).

508 3. Marr, D. A theory of cerebellar cortex. *J Physiol* **202**, 437-470 (1969).
509 4. Ito, M., Sakurai, M. & Tongroach, P. Climbing fibre induced depression of both mossy
510 fibre responsiveness and glutamate sensitivity of cerebellar Purkinje cells. *J Physiol* **324**, 113-
511 134 (1982).
512 5. Ekerot, C.F. & Kano, M. Long-term depression of parallel fibre synapses following
513 stimulation of climbing fibres. *Brain Res* **342**, 357-360 (1985).
514 6. Tank, D.W., Sugimori, M., Connor, J.A. & Llinas, R.R. Spatially resolved calcium dynamics
515 of mammalian Purkinje cells in cerebellar slice. *Science* **242**, 773-777 (1988).
516 7. Llinas, R. & Sugimori, M. electrophysiological properties of in vitro purkinje cell somata
517 in mammalian cerebellar slices. *J. Physiol.*, 171-195 (1980).
518 8. Medina, J.F., Nores, W.L., Ohyama, T. & Mauk, M.D. Mechanisms of cerebellar learning
519 suggested by eyelid conditioning. *Current opinion in neurobiology* **10**, 717-724 (2000).
520 9. Ohyama, T.N.W.M.M. & Mauk, M. What the cerebellum computes. *Trends in*
521 *Neurosciences* **26**, 222-227 (2003).
522 10. Raymond, J.L., Lisberger, S.G. & Mauk, M.D. The cerebellum: a neuronal learning
523 machine? *Science* **272**, 1126-1131 (1996).
524 11. Schultz, S.R., Kitamura, K., Post-Uiterweer, A., Krupic, J. & Hausser, M. Spatial pattern
525 coding of sensory information by climbing fiber-evoked calcium signals in networks of
526 neighboring cerebellar Purkinje cells. *J Neurosci* **29**, 8005-8015 (2009).
527 12. Tsutsumi, S.*, et al.* Structure-function relationships between aldolase C/zebrin II
528 expression and complex spike synchrony in the cerebellum. *J Neurosci* **35**, 843-852 (2015).
529 13. Ozden, I., Dombeck, D.A., Hoogland, T.M., Tank, D.W. & Wang, S.S. Widespread state-
530 dependent shifts in cerebellar activity in locomoting mice. *PLoS One* **7**, e42650 (2012).
531 14. De Gruijl, J.R., Hoogland, T.M. & De Zeeuw, C.I. Behavioral correlates of complex spike
532 synchrony in cerebellar microzones. *J Neurosci* **34**, 8937-8947 (2014).
533 15. Tang, T., Suh, C.Y., Blenkinsop, T.A. & Lang, E.J. Synchrony is Key: Complex Spike
534 Inhibition of the Deep Cerebellar Nuclei. *Cerebellum* **15**, 10-13 (2016).
535 16. Lee, K.H.*, et al.* Circuit mechanisms underlying motor memory formation in the
536 cerebellum. *Neuron* **86**, 529-540 (2015).

537 17. Histed, M.H., Carvalho, L.A. & Maunsell, J.H. Psychophysical measurement of contrast
538 sensitivity in the behaving mouse. *J Neurophysiol* **107**, 758-765 (2012).
539 18. Chettih, S.N., McDougle, S.D., Ruffolo, L.I. & Medina, J.F. Adaptive timing of motor
540 output in the mouse: the role of movement oscillations in eyelid conditioning. *Front Integr*
541 *Neurosci* **5**, 72 (2011).
542 19. Gaffield, M.A., Amat, S.B., Bito, H. & Christie, J.M. Chronic imaging of movement-related
543 Purkinje cell calcium activity in awake behaving mice. *J Neurophysiol* **115**, 413-422 (2016).
544 20. Mukamel, E.A., Nimmerjahn, A. & Schnitzer, M.J. Automated analysis of cellular signals
545 from large-scale calcium imaging data. *Neuron* **63**, 747-760 (2009).
546 21. Najafi, F., Giovannucci, A., Wang, S.S. & Medina, J.F. Coding of stimulus strength via
547 analog calcium signals in Purkinje cell dendrites of awake mice. *Elife* **3**, e03663 (2014).
548 22. Ozden, I., Lee, H.M., Sullivan, M.R. & Wang, S.S. Identification and clustering of event
549 patterns from in vivo multiphoton optical recordings of neuronal ensembles. *J Neurophysiol*
550 **100**, 495-503 (2008).
551 23. Ozden, I., Sullivan, M.R., Lee, H.M. & Wang, S.S. Reliable coding emerges from
552 coactivation of climbing fibers in microbands of cerebellar Purkinje neurons. *J Neurosci* **29**,
553 10463-10473 (2009).
554 24. Najafi, F., Giovannucci, A., Wang, S.S. & Medina, J.F. Sensory-driven enhancement of
555 calcium signals in individual Purkinje cell dendrites of awake mice. *Cell Rep* **6**, 792-798 (2014).
556 25. Najafi, F. & Medina, J.F. Beyond "all-or-nothing" climbing fibers: graded representation
557 of teaching signals in Purkinje cells. *Front Neural Circuits* **7**, 115 (2013).
558 26. Yang, Y. & Lisberger, S.G. Purkinje-cell plasticity and cerebellar motor learning are
559 graded by complex-spike duration. *Nature* **510**, 529-532 (2014).
560 27. Kitamura, K. & Hausser, M. Dendritic calcium signaling triggered by spontaneous and
561 sensory-evoked climbing fiber input to cerebellar Purkinje cells in vivo. *J Neurosci* **31**, 10847-
562 10858 (2011).
563 28. Konnerth, A., Dreessen, J. & Augustine, G.J. Brief dendritic calcium signals initiate long-
564 lasting synaptic depression in cerebellar Purkinje cells. *Proc Natl Acad Sci U S A* **89**, 7051-7055
565 (1992).

566 29. Miyakawa, H., Lev-Ram, V., Lasser-Ross, N. & Ross, W.N. Calcium transients evoked by
567 climbing fiber and parallel fiber synaptic inputs in guinea pig cerebellar Purkinje neurons. *J*
568 *Neurophysiol* **68**, 1178-1189 (1992).
569 30. Eilers, J., Augustine, G.J. & Konnerth, A. Subthreshold synaptic Ca2+ signalling in fine
570 dendrites and spines of cerebellar Purkinje neurons. *Nature* **373**, 155-158 (1995).
571 31. Hartell, N.A. Strong activation of parallel fibers produces localized calcium transients
572 and a form of LTD that spreads to distant synapses. *Neuron* **16**, 601-610 (1996).
573 32. Apps, R. & Garwicz, M. Anatomical and physiological foundations of cerebellar
574 information processing. *Nat Rev Neurosci* **6**, 297-311 (2005).
575 33. Ohmae, S. & Medina, J.F. Climbing fibers encode a temporal-difference prediction error
576 during cerebellar learning in mice. *Nat Neurosci* **18**, 1798-1803 (2015).
577 34. Ackerley, R., Pardoe, J. & Apps, R. A novel site of synaptic relay for climbing fibre
578 pathways relaying signals from the motor cortex to the cerebellar cortical C1 zone. *J Physiol*
579 **576**, 503-518 (2006).
580 35. Kitazawa, S., Kimura, T. & Yin, P.B. Cerebellar complex spikes encode both destinations
581 and errors in arm movements. *Nature* **392**, 494-497 (1998).
582 36. Zhou, H.*, et al.* Cerebellar modules operate at different frequencies. *Elife* **3**, e02536
583 (2014).
584 37. Paukert, M., Huang, Y.H., Tanaka, K., Rothstein, J.D. & Bergles, D.E. Zones of enhanced
585 glutamate release from climbing fibers in the mammalian cerebellum. *J Neurosci* **30**, 7290-7299
586 (2010).
587 38. Blenkinsop, T.A. & Lang, E.J. Synaptic action of the olivocerebellar system on cerebellar
588 nuclear spike activity. *J Neurosci* **31**, 14708-14720 (2011).
589 39. Bengtsson, F., Ekerot, C.F. & Jorntell, H. In vivo analysis of inhibitory synaptic inputs and
590 rebounds in deep cerebellar nuclear neurons. *PLoS One* **6**, e18822 (2011).
591 40. Person, A.L. & Raman, I.M. Purkinje neuron synchrony elicits time-locked spiking in the
592 cerebellar nuclei. *Nature* **481**, 502-505 (2012).

593 41. McElvain, L.E., Bagnall, M.W., Sakatos, A. & du Lac, S. Bidirectional plasticity gated by
594 hyperpolarization controls the gain of postsynaptic firing responses at central vestibular nerve
595 synapses. *Neuron* **68**, 763-775 (2010).
596 42. Pugh, J.R. & Raman, I.M. Potentiation of mossy fiber EPSCs in the cerebellar nuclei by
597 NMDA receptor activation followed by postinhibitory rebound current. *Neuron* **51**, 113-123
598 (2006).
599 43. Miles, F.A. & Lisberger, S.G. Plasticity in the vestibulo-ocular reflex: a new hypothesis.
600 *Annu Rev Neurosci* **4**, 273-299 (1981).
601 44. Matias, S., Lottem, E., Dugue, G.P. & Mainen, Z.F. Activity patterns of serotonin neurons
602 underlying cognitive flexibility. *Elife* **6** (2017).
603 45. Belova, M.A., Paton, J.J., Morrison, S.E. & Salzman, C.D. Expectation modulates neural
604 responses to pleasant and aversive stimuli in primate amygdala. *Neuron* **55**, 970-984 (2007).
605 46. Hayden, B.Y., Heilbronner, S.R., Pearson, J.M. & Platt, M.L. Surprise signals in anterior
606 cingulate cortex: neuronal encoding of unsigned reward prediction errors driving adjustment in
607 behavior. *J Neurosci* **31**, 4178-4187 (2011).
608 47. Pearce, J.M. & Hall, G. A model for Pavlovian learning: variations in the effectiveness of
609 conditioned but not of unconditioned stimuli. *Psychol Rev* **87**, 532-552 (1980).
610 48. Roesch, M.R., Esber, G.R., Li, J., Daw, N.D. & Schoenbaum, G. Surprise! Neural correlates
611 of Pearce-Hall and Rescorla-Wagner coexist within the brain. *Eur J Neurosci* **35**, 1190-1200
612 (2012).
613 49. Raymond, J.L. & Medina, J.F. Computational Principles of Supervised Learning in the
614 Cerebellum. *Annu Rev Neurosci* **41**, 233-253 (2018).

615

616

617 **Figure Legends**

618

619 **Figure 1**. Cerebellar sensorimotor task for head-fixed mice. Ai) Confocal image of a sagittal
620 section from PCP2-Cre x Arch mouse showing expression of the inhibitory opsin Arch in PCs at
621 low (left) and high (right) resolution. ML; molecular layer, PCL; Purkinje cell layer, GCL; granule
622 cell layer. Aii) Schematics of a cranial window implanted over lobule simplex (left) and

623 configuration for optogenetic stimulation (right). Bi) *Left*, representative single unit recording of
624 PC simple spike raster (top) and spike rate histogram (bottom) aligned to onset of Arch
625 activation (green shaded interval). *Right*, Location of the stimulation sites that evoked ipsilateral
626 forelimb movements (green). Bii) Average normalized firing rates from superficial (top) or deep
627 (bottom) PCs at low (left) or high (right) stimulation powers (n=5 mice; 10-20 mW – superficial:
628 n=6 cells; deep: n=5 cells; 30-50 mW – superficial: n=10 cells; deep: n=4 cells). Note that the
629 lower powers used to map motor responses were only sufficient to strongly suppress neurons
630 above 500 μm. C) Schematic of configuration of behavioral task. Head-fixed mice were trained
631 to release a lever in response to a visual cue, with reward delivered immediately upon correctly
632 timed movement. D) Schematic of trial structure. The delay between lever press and release
633 cue was either randomized (cue reaction) or constant (cue prediction) from trial to trial. E)
634 Average reaction time (from cue onset) as a function of trial number for an example cue reaction
635 session. Each point is the average of 5 trials. F) Same as E, for a cue prediction session. G)
636 Summary of reaction times for all cue prediction sessions with a 0.5 s cue delay (gray; n=44
637 sessions, 10 mice) and all cue reaction sessions (black; n=26 sessions, 7 mice). Error bars are
638 ±SEM across sessions. H) Summary of mean change in reaction time from the beginning to the
639 end of cue prediction and reaction sessions (methods) (n =44 sessions, 0.5 s; n=9, 1.0 s; n=6,
640 1.5 s; n=30, 2.0 s; n=26, Δt). One-way ANOVA, main effect of cue delay, F=10.72, df=3. Error
641 bars are ± SEM across sessions. I) *Top*, average lever kinematic traces from an example 0.5 s
642 cue prediction session aligned to the cue show that lever releases occur sooner in the last 1/3 of
643 trials (black, n=149) as compared to the first 1/3 of trials (gray, n=149). Shaded area is ±SEM
644 across trials. *Bottom,* same example session as above aligned separately to press and release
645 showing no difference in kinematics from beginning (gray) to end (black) of the session. J)
646 Summary of average lever release times (20-80% rise time) across sessions (n=15 sessions, 4
647 mice)
648
649 **Figure 2**. Learning requires synaptic transmission in lobule simplex. A) Average lever
650 kinematic traces from an example 0.5 s cue prediction session after application of NBQX (300
651 μM), CPP (30 μM) and MCPG (30 μM). *Top*, traces aligned separately to press and release
652 showing no difference in kinematics from beginning (blue, first 1/3 of trials, n=190) to end (black,
653 last 1/3 of trials, n=190) of the session. *Bottom*, traces aligned to the cue show that lever
654 releases do not occur sooner in the last 1/3 of trials (black) as compared to the first 1/3 of trials
655 (blue). Shaded area is ±SEM across trials. B) Summary of average lever release times (20-80%
656 rise time) across NBQX 0.5s cue prediction sessions (n=14 sessions, 6 mice). C) Summary of

657 mean reaction time for all 0.5 s cue prediction sessions where NBQX (n=14) CPP (n=14) and
658 MCPG (n=8) were applied locally to LS (blue; n=6 mice) compared to summary of cue reaction
659 sessions (black; replotted from Fig 1G). Error bars are ± SEM across sessions. D) Summary of
660 mean change in reaction time from the beginning to the end of NBQX 0.5s cue prediction
661 sessions (blue; n=10 sessions, 6 mice) compared to cue prediction and reaction sessions
662 (replotted from Fig. 1H). Error bars are ± SEM across sessions.
663
664 **Figure 3.** Single photon imaging during cue reaction sessions. A) Example ΔF/F single trial
665 timecourses for a correctly timed lever release (left) and an early lever release (right). RW =
666 reward, delivered immediately on correct release. B) Field of view (images separated by 100
667 ms) showing the average fractional change in fluorescence aligned to lever release for correct
668 (top) and early (bottom) trials from an example session (same session as example from A). C)
669 Calcium transient timecourses averaged across 87 trials from the experiment in A. B) for correct
670 (black) and early trials (red). Error bars are ±SEM across trials. D) Summary of the mean peak
671 calcium transients (measured on single trial basis, methods) for all correct and early trials
672 across sessions (n=10 animals, 17 sessions). Colors represent different animals, and each
673 point represents an imaging session. Note that all points lie below the diagonal. *Inset*, schematic
674 of ROIs for all sessions. Outline color corresponds to mouse from scatter plot, and fill color
675 indicates imaging depth identified by post-hoc histology. Error bars are ± SEM across sessions.
676
677 **Figure 4**. Lever dynamics and licking do not explain differences in complex spiking across trial
678 types. A) Average lever kinematics across 385 trials from a representative cue reaction
679 session for correct (black) and early (red) trials aligned to threshold crossing for both press and
680 release. B) Summary of rise times for press (left) and release (right) on correct and early trials
681 across sessions (n=14 sessions, 3 mice). C) Average timecourse of licking for correct (top) and
682 early (bottom) release trials across sessions (n=15 sessions, 9 mice). Error bars are ±SEM
683 across sessions. D) Two example sessions (top, n=198 trials, bottom, n=173 trials) illustrating
684 the relationship between release-evoked calcium transients (black and red lines) and licking
685 (blue bars) for correct (left) and early (right) release trials. Error bars are ± SEM across trials. E)
686 Summary of the relationship between lick rates and the magnitude of fluorescent transients for
687 correct (black) and early (red) release trials (n= 15 sessions, 9 mice). Error bars are ±SEM
688 across trials. F) Summary of the mean ratio of early and correct trial-evoked peak calcium
689 transient and lick rates for the same sessions in E. G) Summary of the Spearman's correlation

690 (ρ) between lick rate and peak ΔF/F on correct (black) and early (red) lever releases across
691 trials for each session (n=8 sessions, 7 animals). Filled circles are mean and SEM across
692 sessions.
693
694 **Figure 5**. Complex spiking produces larger mean response in individual dendrites and
695 enhanced population responses when movement is correctly timed. A) *Left*, average GCaMP
696 fluorescence from an example 2-photon imaging session (30 Hz acquisition rate). Scale bar =
697 100 μm. *Middle*, pixel mask of individual PC dendrites extracted from the same session. Right,
698 average calcium responses measured from the highlighted dendrite segregated by trial event
699 (n=186 trials). Dotted line represents time of lever press (blue) or lever release (correct: black;
700 early: red). Shaded area is ±SEM across trials. B) Left, average timecourse of calcium response
701 for all significantly responsive dendrites aligned to lever press (blue), or release (correct
702 releases (black), early releases (red), and too-fast releases (green) that occurred < 200 ms
703 following the visual cue; n=17 animals, 30 sessions, 1146 dendrites). Shaded area is ±SEM
704 across dendrites. *Middle*, summary scatter plot comparing the average peak amplitude of the
705 calcium transient for each significantly responsive PC dendrite (gray) and the average of all
706 dendrites (red) for correct and early release trials. P-value from paired t-test. *Right*, same as
707 middle for correct and too fast release trials. P-value from paired t-test. C) Pixel masks of
708 dendrites significantly responsive to lever release on correct trials, lever release on early trials,
709 and lever press for the example session in A. Color map represents average ΔF/F. D) Summary
710 across experiments of the fraction of dendrites responsive to correct lever releases vs early
711 releases (top, left), to only correct or only early releases (top, right), to lever press vs release
712 (bottom, left), and only to press or release (bottom, right). Responses were categorized as
713 significant ($p<0.05$) according to a one-tailed t-test (methods). E) *Left,* average amplitude of
714 correct and early release-evoked calcium events for all dendrites normalized to the amplitude of
715 spontaneous calcium events. One-way ANOVA, F=1.8, df=2. *Right,* mean spontaneous (gray,
716 n=286,964 events, 1146 dendrites) and correct (black, n=19,550 events, 1146 dendrites) and
717 early (red, n=9,167 events, 1146 dendrites) release lever-evoked calcium events across all
718 responsive dendrites. Error bars are ±SEM across dendrites.
719
720 **Figure 6**. Complex spiking occurs with higher peak rates and greater synchrony when
721 movements are correctly timed. A) Peri-release time histogram of calcium events on correct
722 (black) and early (red) release trials (n=17 animals, 30 sessions, 1146 dendrites). Bin width = 33
723 ms. Shaded area is ±SEM across dendrites. B) Summary of average event rate for correct and

724 early releases for each session (n=30). Error bars are ±SEM across dendrites. C) Same as B for
725 average event latency relative to release for each session (n=30). Error bars are ±SEM across
726 dendrites. D) Summary of average standard deviation (S.D.) of event times across trials within
727 single dendrites for each session (n=30). Error bars are ±SEM across dendrites. E) Same as D
728 for measurement of S.D. of event times across dendrites for each session (n=30). Open circles
729 are statistically significant for reduced correct trial jitter across dendrites (paired t-test). Error
730 bars are ±SEM across trials. F) Summary of the average S.D. of event times when aligned to
731 either lever release or visual cue for each session (n=30). Error bars are ±SEM across
732 dendrites. G) Summary of the average latency to peak event probability relative to cue (gray
733 circles) or lever release (black circles) compared with the average session reaction time for
734 each session (n=30). X-error bars are ±SEM across trials; Y-error bars are ±SEM across
735 dendrites.
736
737 **Figure 7**. Complex spiking is correlated across parasagittal zones, with higher correlations on
738 correct lever releases. A) *Left*, Average GCaMP fluorescence for three example experiments.
739 ROIs from lobule simplex (white boxes) were selected for unsupervised clustering analysis
740 (meta K-means, methods). *Right*, pixels are colored according to cluster identity for each
741 example experiment. M=medial, R=rostral, C=caudal, L=lateral. Note the alignment of the
742 clustered zones along the rostro-caudal axis. B) Within cluster correlations (n=6 clusters,
743 Pearson's) between correct and early lever release trials from an example session in A (bottom)
744 for each of the identified clusters (yellow). C) Summary of average Pearson's correlation
745 coefficient for all pixel pairs (methods) within clusters (n = 39) across experiments for correct
746 and early release trials (n=5 animals, 7 sessions, 39 clusters). Colors denote clusters from the
747 same session. D) Summary of the relationship between peak ΔF/F and Pearson's correlation
748 coefficients for paired correct (black) and early (red) trials for each cluster (n=39). Linear fits
749 were performed for within cluster correlations using correct and early trials separately. E)
750 Same as C for pairs of pixels across neighboring clusters (n=31 cluster pairs). F) Same as C for
751 pairs of pixels across non-neighboring clusters (n=50 cluster pairs).
752
753 **Figure 8.** Complex spiking is modulated by learned sensorimotor predictions. A) Top, Average
754 calcium transient in response to unexpected reward (green, aligned to first lick) and correct
755 lever releases (black, aligned to release). Shaded error is SEM across dendrites (n=120).
756 Bottom, Average lick rate for unexpected reward and correct lever releases. Error is SEM
757 across sessions (n=3). B) Summary of the mean peak calcium transients in a 500 ms window at

758 the time of release (methods) across all 2-photon experiments for correct (black) and early (red)
759 release trials binned according to hold time (250ms bins). Linear fits were applied to data from
760 each trial type (n=17 animals, 30 sessions). Error bars are SEM across sessions. C) Mean
761 timecourse of calcium transients for an example session (n=43 dendrites) divided according to
762 early trials with hold durations of < 1.0s (red) and > 3.5s (dark red). Note the late, second
763 response for long hold duration trials. Shaded error is SEM across dendrites. D) Single trial
764 example timecourses from an individual dendrite from the session in C. Gray bars represent
765 analysis windows for subsequent plots E-G) Summary of peak calcium transients measured in
766 the shaded windows from D for all dendrites (n=1146) according to lever hold time (E,F) and
767 trial outcome (G). P-values represent paired t-tests. H) Mean calcium transient timecourses
768 averaged across all dendrites (n=1146) on short and long hold early release trials. Shaded error
769 is SEM across dendrites. I) Mean lick rates for the subset of experiments where licking was
770 measured in H (n= 6 animals, 10 sessions)). Error bars are SEM across sessions. J) Example
771 timecourses of mean calcium transients from a single session (n=22 dendrites) for correct
772 (black), and reward omission (dark blue) trials. Note the late, second response on omission
773 trials. Shaded error is SEM across dendrites. K) Single trial example timecourses from an
774 individual dendrite from the session in J. L-M) Summary of peak calcium transients measured in
775 the shaded windows in K on correct and reward omission lever trials (n=81 dendrites, 3 animals,
776 3 sessions). P-values represent paired t-tests. N) Mean timecourses of calcium transients
777 averaged across all dendrites (n=81) for correct (black) and reward omission (dark blue) trials.
778 Vertical bars represent the lick rate averaged across trials for all reward omission sessions.
779 Shaded error is SEM across dendrites. Error bars are SEM across sessions.
780
781 **Supplemental Figures**
782 **Figure 1.** Mapping of motor output driven by Arch and electrical stimulation of superficial
783 cerebellar cortex. A) Schematics of the results of Arch stimulation over a grid of sites in lobule
784 simplex (Sim) and Crus I for all five mice. Colors denote outcome of stimulation. B) Same as A
785 for three mice tested with electrical microstimulation.
786
787 **Figure 2**. Retention and extinguishment of learning for cue prediction regime. A) Average
788 reaction times relative to cue for the first (left) and second (right) sessions where animals
789 performed 0.5 s cue prediction on consecutive training days (n=17 sessions, 5 mice). Error bars
790 are ±SEM across sessions. B) Same as A for 2 s cue prediction sessions (n=10 sessions, 6
791 mice). C) *Left,* example cumulative distributions of reaction times for cue reaction sessions

792 immediately surrounding a cue prediction session (session 0). Trials from the cue prediction
793 session include only the last 1/3 of the session when the animal was anticipating the cue timing.
794 *Right,* summary of distribution skewness across cue reaction sessions immediately surrounding
795 cue prediction sessions (n=43 sessions). Error bars are SEM across sessions. D) Same as A
796 for pairs of 0.5 s prediction sessions separated by 3 or more cue reaction sessions (n=20
797 sessions, 10 mice).
798
799 **Figure 3**. Performance in the cue prediction condition in control and NBQX sessions. A-E)
800 Summary across experiments of mean percent correct lever releases, mean baseline reaction
801 time from the visual cue, mean reaction time variance, mean duration to press, mean number of
802 trials performed, and the mean duration of behavioral sessions. n=44 sessions, 0.5 s; n=9, 1.0
803 s; n=6, 1.5 s; n=30, 2.0 s; n=26, Δt; n=14, 0.5 s NBQX. Error bars are SEM across sessions.
804 For each cue delay, the minimum and maximum (x,y) number of trials performed in single
805 sessions was: 0.5 s: (309, 700) 1 s: (252, 900) 1.5 s: (202, 775) 2 s: (278,1185) Δt: (313, 772)
806 0.5 s NBQX: (227, 429). F_i) Individual (top) and average (bottom) lever trajectories aligned to
807 lever press (left) and release(right) segregated by duration into quartiles (n=112 trials / quartile)
808 for a representative 0.5 s cue prediction session. F_{ii}) Same as F_i for a representative 0.5 s cue
809 prediction session in NBQX. (n=142 trials / quartile). G) Summary of press (left) and release
810 (right) quartiles across experiments for control (top; n=15 sessions) and NBQX (bottom; n=14
811 sessions) experiments. H) Summary of the ratio between press and release ranges (difference
812 between 1st and 4th quartile) for control (black) and NBQX (blue) experiments.
813
814 **Figure 4.** Pharmacological modulation of complex spiking in lobule simplex. A) Single unit
815 recordings during NBQX application to LS. Top, summary of complex spike rates in control and
816 after application of NBQX for individual cells (black; n=9 cells, 5 mice) and the average of all
817 cells (red). Error bars are ±SEM across cells. Bottom, same as top for simple spike rates. Note
818 that NBQX strongly reduces complex but not simple spike rates. B) (top) Raw epifluorescence
819 images from parasagittal cerebellar sections showing fluorescein labeling after surface
820 application to lobule simplex *in vivo* (methods, 3 mice). (bottom) Pixel masks from the same
821 images above. Pixels were thresholded at 30% of maximum value to visualize and quantify
822 fluorescein labeling. C) Summary of mediolateral fluorescein spread across sections. (n=3
823 animals). Error bars are SEM across animals.
824

825 **Figure 5**. Segmentation of PC dendrites from imaging experiments. A) Example single photon
826 imaging field of view (left) is segmented to mask individual dendrites (right) used for subsequent
827 single cell analysis. Scale bar = 100 μm. B) Example timecourse of raw fluorescence (top) from
828 the circled dendrite in A showing individual calcium transients identified (gray circles) according
829 to peaks in the first derivative of the fluorescence trace (bottom). C) Same as A for an example
830 two photon field of view. Note that while PC somata are visible (round, top right), image
831 segmentation does not extract activity from these structures. Scale bar = 100 μm. D) Same as
832 B for the experiment in C. E) Top, example time course of a single unit PC recording from an
833 awake mouse illustrating detection of complex spikes (gray circles). Bottom, overlay of
834 individual simple (left) and complex (right) spike waveforms (gray) and the average waveform
835 (black). F) Summary of mean spike rates ± SEM across all two photon dendrite imaging
836 sessions (blue; n=1146 dendrites) and acute single unit recordings (n=11 units).
837
838 **Figure 6**. Single unit PC recordings of complex spiking during the cue prediction condition. A)
839 Top, Schematic of the trial structure schematic, where a constant cue delay of 500ms was
840 imposed on each trial. Middle top, Average simple (SS, left) and complex (CS, right) spike
841 waveforms from an example single unit. Middle bottom, Histogram of SS firing rate aligned to
842 complex spike time revealing post-CS pause, confirming isolation of single PC. Bottom, raster of
843 single trial complex spikes and session PSTH aligned to lever release. B) Single trial voltage
844 traces (complex spikes- open blue circle) from the cell in A aligned to lever release (correct-
845 black circle; early- red circle). C) Expansion of 5 consecutive traces from B at time of lever
846 release. D) Mean normalized complex spike rate (methods) from single unit recordings (31 PCs,
847 8 mice) aligned to lever release for correct (black) and early (red) trials during the cue prediction
848 condition. Shaded error is SEM across PCs. E). Mean normalized complex spike rates aligned
849 to cue presentation for the first 1/3 of trials (black) and the last 1/3 of trials (orange) across cue
850 prediction sessions for correct (left) and early (right) trials (31 PCs, 8 mice). Shaded error is
851 SEM across PCs. F) Summary of the S.D. of spike times when aligned to either lever release or
852 visual cue for each PC (n=31). P-values reflect paired t-tests.
853
854 **Figure 7.** Differential complex spiking on correct and early release trials is not driven by motor
855 signals due to licking. A) Example imaging data from an inter-trial interval (ITI) showing a lick
856 responsive dendrite (top, dark blue) and a lick unresponsive dendrite (bottom, black) in the
857 same field of view. B) Averaged lick triggered calcium transients for the lick responsive dendrite
858 (dark blue) and a lick unresponsive dendrite (black) in A). n=28 licks, Error bars are SEM across

859 lick-triggered events. C) Mean lick triggered calcium transient across all lick responsive (dark
860 blue) and lick unresponsive (black) dendrites. Shaded error is SEM across dendrites. D)
861 Summary of the Spearman's correlation between lick rate and amplitude of the calcium transient
862 in each frame across trials for lick responsive (dark blue) and lick unresponsive dendrites (grey).
863 Red points indicate the mean ± SEM across dendrites (447 dendrites, 6 animals and 10
864 sessions). E) Summary comparing the amplitude of calcium transients for lick responsive
865 neurons only in response to either a single lick (blue) or a lick bout (3 or more licks with ≤ 300
866 ms between licks; cyan). Note that additional licking does not produce larger responses. F)
867 Summary comparing the amplitude of calcium transients on correct (black) and early (red) lever
868 releases for lick unresponsive dendrites only. G) Same as F, for lick responsive dendrites. P-
869 values reflect paired t-tests.
870
871 **Figure 8.** Example single trial and session average calcium transients from 2-photon imaging.
872 A) Example single trial data from an individual dendrite showing the normalized calcium
873 transient across an early release trial from before lever press to after the lever release. B) Same
874 as A) but for a correct trial, including the time of cue presentation. C) Mean calcium transients
875 across trials (n= 186) for the dendrite in A and B. Error bars are SEM across trials. D) Single
876 trial example, aligned to lever release, showing all dendrites from the experiment illustrated in
877 Fig. 5C on a correct trial over 1 second surrounding release (n=115 dendrites). Lever press is
878 off scale. E) Same as D, but for an early release trial from the same imaging session.
879
880 **Figure 9**. Unexpected reward drives complex spiking in lick unresponsive and responsive
881 dendrites. A-B) Top, Average calcium transient in response to unexpected reward (green,
882 aligned to first lick) and correct lever releases (black, aligned to release). Shaded error is SEM
883 across dendrites. Bottom, Average lick rate for unexpected reward and correct lever releases.
884 Error is SEM across experiments (n=3). Lick responsiveness was defined according to
885 significant responses in the lick triggered averaged taken from the inter-trial interval (Supp. Fig.
886 7). C). Summary of peak calcium transients in the same neurons for correct lever releases vs
887 unexpected reward trials. Note that responses are proportional, and response amplitude is
888 determined by response probability (Fig. 5,6). P-value reflects paired t-test.
889
890 **Figure 10**. Complex spiking scales with lever hold time for early releases in single photon
891 imaging experiments. Summary of peak calcium transients in a 500 ms window at the time of
892 release (methods) across all single photon experiments for correct (black) and early (red)

release trials binned according to hold time (250ms bins). Linear fits were applied to data from each trial type (n=10 animals, 17 sessions). Error bars are SEM across sessions.

Figure 11. Mice have full control over the lever trajectory. A) Individual (top, n=217) and average (bottom, 54 per quartile) lever trajectories aligned to lever press (left) and release (right) for manual lever depression followed by unperturbed gravity return. Shaded error is SEM across trials. B) Summary of press (left) and release (right) quartiles across experiments for manual lever experiments (n=4). Note the lack of variability across quartiles. C) Summary scatterplot comparing 20-80% rise times of lever press and release for experiments where the lever was controlled by mice (black, n=15) and manual press (green, n=4) D) Summary comparison measuring the average difference from the mean of the slowest release quartile and the fastest release quartile for experiments where the lever was controlled by mice (black) and manual press (green). Lever trajectories were sorted according to duration in a window from 200ms before threshold crossing to the time of a threshold crossing half way between the top and bottom of the total lever displacement. The slowest and fastest 25 trials were extracted for comparison, and their average rise time was normalized by subtracting that of the mean trajectory of the whole session. Error bars are SEM across sessions. These results show that mice produce movements both slower and faster than the mean, indicating full control over the lever trajectory.

Video 1. Optogenetic silencing of superficial PCs in lobule simplex drives ipsilateral forelimb movements. An external fiber coupled laser was activated at the time indicated by the green circle above lobule simplex (methods), resulting in forelimb movement.

Video 2. Example correct and early release trials from the cue prediction condition. Two example trials from the same mouse in the same training session are shown first in real time, and then repeated at 0.25x video rate.

Methods:

<u>Mice</u>

926 All experimental procedures using animals were carried out with the approval of the Duke
927 University Animal Care and Use Committee. All experiments were performed during light cycle
928 using adult mice (>p60) of both sexes, randomly selected from breeding litters. All mice were
929 housed in a vivarium with normal light/dark cycles in cages with 1-5 mice. Imaging experiments
930 were performed using Tg(PCP2-Cre)3555Jdhu mice (Jackson Labs, 010536; n=12).
931 Optogenetic mapping experiments were conducted in PCP2-Cre animals crossed with
932 Ai35(RCL-Arch/GFP) (Jax 012735; n=5 mice). Single unit recordings during the cue prediction
933 condition were performed in wild type C57BL/6J mice (n= 8 mice). Additional behavioral
934 experiments where imaging was not performed were conducted in wild type C57BL/6J mice
935 (n=18). We used two exclusion criteria for animals in this study: (1) poor recovery or other
936 health concerns following surgical intervention or (2) missed virus injection, as determined by *in*
937 *vivo* imaging and post-hoc histological analysis.
938
939 Surgical Procedures
940 3-10 hours prior to surgery, animals received dexamethasone (3mg/kg) and ketoprofen
941 (5mg/kg). Surgical procedures were performed under anesthesia, using an initial dose of
942 ketamine/xylazine (50mg/kg and 5mg/kg) 5 minutes prior to surgery and sustained during
943 surgery with 1.0-2.0% isoflurane. Toe pinches and breathing were used to monitor anesthesia
944 levels throughout surgeries. Body temperature was maintained using a heating pad (TC-1000
945 CWE Inc.). Custom-made titanium headplates (HE Parmer) were secured to the skull using
946 Metabond (Parkell). For imaging experiments, a 3mm diameter craniotomy was made over the
947 lobule simplex approximately 1.4mm lateral and 2.8mm posterior to lambda, and glass cover
948 slips consisting of two 3mm bonded to a 5mm coverslip (Warner Instruments No. 1) with index
949 matched adhesive (Norland No. 1) were secured in the craniotomy using Metabond. Buprenex
950 (0.05mg/kg) and cefazolin (50mg/kg) were administered following surgery twice a day for two
951 days. Following a minimum of 4 recovery days, animals were water deprived for 3 days, or until
952 body weight stabilized at 85% of initial weight, and were habituated to head restraint (3-5 days)
953 prior to behavioral training.
954 For imaging experiments, the glass cover slip was removed following behavioral training,
955 and mice were injected (WPI UMP3) with AAV1.CAG.Flex.GCaMP6f.WPRE.SV40 (UPenn
956 vector core, titer = 9.40×10^{12} or 7.60×10^{12}). 150 nL virus diluted 1:1-1:5 in ACSF was injected at a
957 rate of 30nl/min and a depth of 150 μm at 1-3 sites in dorsal lobule simplex. Imaging was
958 performed beginning 14 days following injection.

959 For *in vivo* pharmacology experiments, a 3mm craniotomy was performed over lobule
960 simplex of headposted mice, and the dura mater was peeled back at the center of the
961 craniotomy. 10uL of combined NBQX (300 μM) and CPP (30 μM) was applied into a well
962 surrounding the craniotomy on the surface of the cerebellum 20 minutes prior to behavioral
963 training. In 8 of 14 experiments, MCPG (30 μM) was also included to block metabotropic
964 glutamate receptors. Because there no significant differences in performance across these two
965 groups, all data were pooled for analysis. During behavior, a second drug application of 10uL
966 was administered 20 and 40 minutes into the task, and depending on the duration of training, a
967 third dose was applied after 1 hour. Craniotomies were subsequently covered with silicone
968 elastomer (WPI, Inc.) prior to returning animals to their home cage. To quantify the spread of
969 pharmacological agents in the cerebellum, 10 μL of fluorescein dye (Sigma-Aldrich #F6377,
970 1mM in aCSF) was applied to the craniotomy in 3 animals with the same method and
971 timecourse as for drug applications. Following standard histological processing and imaging
972 (below), labeling was quantified by creating a binary pixel mask thresholded at 30% of the
973 maximum fluorescence value for each experiment. Dye labeling was then measured using the
974 area of these pixel masks (Supp. Fig. 4 B,C).
975
976 Behavior
977 During behavioral training, animals were head-fixed and placed in front of a computer monitor,
978 lever and reward delivery tube. Animals were trained to self-initiate trials by depressing the lever
979 using their right forepaw, and required to successfully hold the lever in the down position for
980 randomized intervals ranging between 500ms and 5 s on the cue reaction paradigm before
981 performing the cue prediction paradigm. For both paradigms, a high contrast hold cue was
982 present at all times, including the intertrial interval (ITI), and transitioned 90 degrees to the
983 release cue on each trial at the instructed time of release until the animal either released the
984 lever or 1 second had passed. Training sessions lasted for 90 minutes, and learning in the cue
985 prediction task occurred with the range of 309-700 trials. Lever releases within one second of
986 the release cue were rewarded immediately at the time of lever release (0.01 M saccharine).
987 Immediately following any lever release, a solenoid was engaged to prevent lever press during
988 the ITI. Following the ITI (3-6 s), the solenoid is lowered, allowing the mouse to self-initiate a
989 new trial. During training, a 1-3 second 'timeout' was implemented to punish early lever
990 releases. No timeouts were used in fully trained animals for imaging or behavior data collection
991 sessions. For reward omission sessions, 20% of randomly determined correct lever releases
992 were unrewarded. Animals used for imaging experiments performed the cue reaction condition

993 with a mean peak percent correct of 79.7 ± 0.23% achieved in 26 ± 2 training days. On imaging
994 days animals performed a range of 150 to 580 trials per session with a mean of 273.9 ±13.1
995 trials. Behavioral parameters including lever press, lever release and licking were monitored
996 using Mworks (http://mworks-project.org) and custom software written in MATLAB (Mathworks).
997 To assess the degree of lever control by the mice, the dynamics of lever press and release
998 trajectories were compared to lever presses initiated by the experimenter where the lever was
999 allowed to return to the rest position on its own (Supp. Fig. 11). These results demonstrate that
1000 mice moved the lever both faster and slower than its intrinsic kinematics, and thus had full
1001 control over its trajectory. Licking was measured with electrical contact circuit. Inter-trial intervals
1002 ranged from 3 to 5 seconds.
1003
1004 Calcium Imaging
1005 *Wide-field imaging*: Single photon imaging was performed using a customized microscope
1006 (Sutter SOM) affixed with a 5x objective (Mitutoyo, 0.14NA) and CMOS camera (Qimaging,
1007 Rolera em-c^2). Excitation (470 nm) was provided by an LED (ThorLabs, M470L3), and data
1008 were collected through a green filter (520-536 nm band pass, Edmund Optics) at a frame rate of
1009 10Hz, with a field of view of 3.5x3.5mm at 1002x1004 pixels.
1010
1011 *Two-Photon Imaging*: Two-photon imaging was performed with a resonant scanning
1012 microscope (Neurolabware) using a 16x water immersion objective (Nikon CFI75 LWD 16xW
1013 0.80NA). Imaging was performed using a polymer to stabilize the immersion solution
1014 (MakingCosmetics, 0.4% Carbomer 940). A Ti:Sapphire laser tuned to 920nm (Spectra Physics,
1015 Mai Tai eHP DeepSee) was raster scanned via a resonant galvanometer (8 kHz, Cambridge
1016 Technology) onto the brain at a frame rate of either 30 Hz with a field of view of either 1030 μm
1017 x 581 μm (796 x 264 pixels) or 555 μm x 233 μm (796 x 264 pixels), or 15.5Hz with a field of
1018 view of 555 μm x 452 μm and (796 x 512 pixels). Data were collected through a green filter (510
1019 ± 42 nm band filter (Semrock)) onto GaAsP photomultipliers (H10770B-40, Hamamatsu) using
1020 Scanbox software (Neurolabware). A total of 12 mice were used for imaging experiments (10
1021 mice for wide-field, 11 mice for two-photon, 12 mice total).
1022
1023 Single Unit Recordings and Optogenetics
1024 Acute single unit recordings were performed in awake animals by performing a craniotomy over
1025 lobule simplex and inserting a multi-electrode silicone probe (Neuronexus, A4x8-5mm-100-400-
1026 177-A32, 4 shanks, 8 site/shank at 100 μm spacing) using a Cerebus multichannel acquisition

1027 system (Blackrock Microsystems, Salt Lake City). For single unit recordings obtained in the cue
1028 prediction condition (Supp. Fig. 6), chronically implanted electrode arrays were used (Dual drive
1029 movable electrode bundles with 8 tungsten electrodes (23 μm) in each cannula or 16 tungsten
1030 electrodes bundle in one cannula, Innovative Neurophysioloy Inc). Electrode arrays were
1031 implanted using stereotaxic coordinates to target lobule simplex at AP 6.2; ML 2.0. Electrode
1032 bundles were inserted into lobule simplex at a depth of approximately 0.2-0.3 mm. The implant
1033 was encased in Metabond for stability.
1034 For both recording conditions, continuous recording data was bandpass filtered with a 2-
1035 pole Butterworth between 250 Hz and 5 kHz and referenced against an electrode with no spikes
1036 using Spike2. Single units were isolated by amplitude thresholding. Template waveforms were
1037 defined and characterized by their width and peak, and PCA of waveforms was done in off-line
1038 in Spike2.
1039 Complex spikes and simple spikes were discriminated as in de Solages et al.[50], first on
1040 the basis of their stereotypical waveform. Complex spikes typically had a multi-wavelet form,
1041 including a large positive peak within 6ms following spike initiation. Manual identification of 10-
1042 20 complex spikes was used to generate a mean template waveform, which was then compared
1043 to all other spikes for a given unit using the Spearman rank order correlation coefficient. The
1044 combination of Spearman coefficients and the magnitude of the positive waveform deflection
1045 was used to segregate complex and simple spikes. The presence of a post-complex spike
1046 pause (20 ms or more) in simple spike firing was verified by cross-correlogram for all isolated
1047 single units.
1048 Complex spike rates for the cue prediction condition were normalized to the baseline firing rate
1049 determined in a one-second window during the ITI according to: (FR-baseline)/baseline) (Supp.
1050 Fig. 6).
1051 For optogenetic mapping of the dorsal cerebellum, an optical fiber (0.39 NA, 400 μm
1052 core multimode, ThorLabs FT400EMT) coupled to a 532 nm laser (Optoengine, MGL-III-532)
1053 was positioned above the cranial window using a micromanipulator (Scientifica PatchStar).
1054
1055 Histology
1056 Mice were deeply anesthetized with ketamine/xylazine (200mg/kg & 30mg/kg respectively, IP)
1057 then perfused with PBS then 4% paraformaldehyde. 100um sagittal sections were cut using a
1058 vibratome (Pelco 102). Cerebellar slices were then mounted using a mounting medium
1059 (Southern Biotech Fluoromount-G or DAPI Fluoromount-G) and imaged with a fluorescence
1060 microscope (Nikon Eclipse 80i).

Data Analysis and Statistics

Behavior: Behavior sessions were only analyzed within the time range of active task performance. Accordingly, the last trial of each session was determined by the occurrence of either two consecutive failed trials (in which the mouse did not release the lever in response to the cue) or two consecutive trials with post-ITI duration to press longer than 1.5x the session average.

Reaction times were measured using lever releases within the reward window as well as those occurring 200ms prior to the reward cue to account for predictive responses. Reaction times are plotted as a binned average of five trials. Initial reaction times were calculated according to the y-intercept of the linear regression of the first fifty trials. Final reaction time at the end of each session was calculated by averaging the reaction times of trials 200-250.

The symmetry of reaction time data about the sample mean was measured to test the extinguishment of learning after following cue prediction sessions according to skewness. Sample skewness was defined by

$$s = \frac{E(\mu - X)^3}{\sigma^3}$$

where μ is the mean of X, $E(*)$ is the expected value of the quantity $*$, and σ is the standard deviation of X. Thus, for a given sample x, this calculates:

$$\frac{\frac{1}{n}\sum_{i=1}^{n}(x_i - \bar{x})^3}{\left(\sqrt{\frac{1}{n}\sum_{i=1}^{n}(x_i - \bar{x})^2}\right)^3}$$

for $x_i \in x$, where $\bar{x}$ is the sample mean.

Movement trajectories were measured using a lever affixed to a rotary encoder (US Digital) with a 60mm radius and 1250 pulses per revolution. Encoder values were collected at 1000 Hz, and trajectories were calculated by up-sampling at 200 μs (5000 Hz) using nearest-neighbor interpolation. Pulse number was converted to degrees, and the vertical displacement in millimeters was calculated using the chord length of the leaver displacement angle. 20-80% rise times were calculated using normalized average trajectories. Presses and releases were sorted according to duration in a window from 200ms before threshold crossing to the time of a threshold crossing half way between the top and bottom of the total lever displacement.

1090

1091 *Wide-field imaging:* Imaging analysis were performed using custom MATLAB code. Regions of
1092 interest (ROIs) were selected within empirically defined forelimb movement region of lobule
1093 simplex according to the spread of GCaMP expression. Window location and the lobule identity
1094 were identified according to folia patterns visible through the cranial window, landmarks
1095 recorded during surgery, and post-hoc histology. Baseline fluorescence (F) was measured on a
1096 trial-by-trial basis during the inter-trial interval (ITI) as the mean fluorescence 900 to 200ms
1097 before trial initiation. Normalized fluorescence ($\Delta F/F$) was calculated according to the
1098 cumulative activity within an ROI, or on a pixel by pixel basis. Lever hold times <200ms in total,
1099 or > 1 s after the visual cue were exceedingly rare, and thus excluded from analysis. Lever
1100 releases between 200ms and 1000ms following the visual cue were classified as correct, and
1101 releases prior to visual cue were classified as early. Lever releases ≤200 ms following the visual
1102 cue were considered too fast to be reactions to the cue based on average reaction time
1103 distributions. Peak $\Delta F/F$ was measured on a trial by trial basis in the time window from 100ms
1104 before to 400 ms after lever release. Note that differences in the timing of single trial calcium
1105 transient peaks produce smaller amplitudes for $\Delta F/F$ timecourses as compared to reported peak
1106 $\Delta F/F$ measurements. Spearman's correlation between lick rate and peak $\Delta F/F$ within sessions
1107 was calculated according to the lick rate within 500 ms following each lever release and the
1108 peak calcium transient for each trial. For this correlation analysis, trials without licking were
1109 removed, and only sessions with 7 or more trials in each condition were included.

1110

1111 *Meta K-means analysis and Cluster Correlations*: Images were first registered to reduce motion
1112 artifacts, and then thresholded at 70% of maximum intensity for each frame to remove
1113 background noise. Images were downsampled 5-fold in both X and Y. Baseline F was defined
1114 as the averaged fluorescence across the entire movie for each pixel, and used to normalize
1115 change in fluorescence ($\Delta F/F$). $\Delta F/F$ was then re-normalized to the maximum $\Delta F/F$ during the
1116 entire movie for each pixel. The repeated k-means clustering algorithm (meta-k-means)
1117 separated pixels to cluster centroids based on a pairwise correlation distance function using
1118 Pearson's linear correlation coefficient (r). The final clusters were determined by first
1119 thresholding all the k-means results at 800 out of 1000 runs, and then by merging highly
1120 correlated clusters based on Dunn's index. Clusters occupying less than 3% of the total imaging
1121 field were excluded from further analysis. Intra-cluster and inter-cluster correlation coefficients
1122 were calculated between 100 ms before and 300 ms after lever release for both correct and
1123 early trials on a frame by frame basis. To test for differences in the relationship between spike

1124 rates and correlation coefficients between trial types, paired clusters from each distribution were
1125 resampled with replacement and fit with a line to measure the y-intercept 1000 times. Statistical
1126 significance was computed according to the 95% confidence interval of the distribution of y-
1127 intercept difference values (difference between y-intercepts 0.0375 ± 0.0013, 95% confidence
1128 interval [0.0349, 0.0402]).
1129
1130 *Two-photon imaging*: Motion in the XY plane was corrected by sub-pixel image registration. To
1131 isolate signals from individual PC dendrites, we utilized principal component analysis (PCA)
1132 followed by independent component analysis (ICA). Final dendrite segmentation was achieved
1133 by thresholding the smoothed spatial filters from ICA. A binary mask was created by combining
1134 highly correlated pixels (correlation coefficient > 0.8) and removing any overlapped regions
1135 between segmented dendrites. Notably, image segmentation using these criteria did not extract
1136 PC soma, which were clearly visible in many single- and two-photon imaging experiments.
1137 Fluorescence changes (ΔF) were normalized to a window of baseline fluorescence (F) between
1138 500ms and 100ms preceding trial initiation. Responses were categorized as significant ($p<0.05$)
1139 according to a one-tailed t-test if the $\Delta F/F$ in a 200 ms window surrounding lever press or
1140 release was larger than that from a 500 ms window immediately preceding lever movement. To
1141 extract events on single trials used for estimation of complex spike rates and event amplitudes,
1142 the first derivative of the raw fluorescence trace was thresholded at 2.5 standard deviations from
1143 baseline. The same methods were used to extract events for the subset of single photon
1144 experiments described in Supp. Fig. 5. For single trial amplitude measurements, only events
1145 well separated in time (greater than 650ms from the next event) were considered; however, for
1146 measurements of rates, all events separated by at least one frame were included. Note that rate
1147 estimates are thus likely to be lower than actual rates, particularly for single photon imaging
1148 where data were collected at 100 ms intervals. For measurements of standard deviation of
1149 event times, events were extracted from a window 433 ms around the lever release, and
1150 independently aligned to the time of visual cue. The same criteria were applied to
1151 electrophysiological measurements of spike times. Event latencies were calculated according to
1152 the time of peak event probability. Peak calcium transients on reward omission trials and on
1153 early release trials were quantified in two time windows (Fig. 8). Window 1 spanned the first
1154 100 ms after lever release, and window 2 spanned 175 ms that began 165ms after lever
1155 release. Spearman's correlation was calculated between lick rate and the peak calcium
1156 transient within sessions on a frame by frame basis for each trial in a window spanning 500 ms
1157 after lever release. Correlation values for correct and early release trials for each dendrite were

averaged separately. Some neurons showed responses to licking, as defined by a mean lick-triggered calcium transient (for dendrites with at least 4 lick events per session) that was significantly larger ($p<0.05$) with respect to baseline (Supp. Fig. 7). Lick triggered averages were constructed from licks presumed to be spontaneous that occurred during the inter-trial interval with a buffer of 1000 ms between the end of the previous trial and the start of analysis to avoid contamination of reward-related licking.

Additional statistics: Data are presented as mean ± S.E.M., unless stated otherwise. Statistical tests were two-sided, except as specifically noted, and analyses of variance (ANOVA) were performed when more than two groups were tested. Differences were considered statistically significant when $P < 0.05$. No correction for multiple comparisons was applied. No statistical methods were used to predetermine sample sizes. Data distribution was assumed to be normal but this was not formally tested. Data collection and analysis were not performed blind to the conditions of the experiments, but data collection relied on automatized measurements and subsequent analysis was based on code uniformly applied across experimental conditions.

Methods-only References

50. de Solages, C., *et al.* High-frequency organization and synchrony of activity in the purkinje cell layer of the cerebellum. *Neuron* **58**, 775-788 (2008).

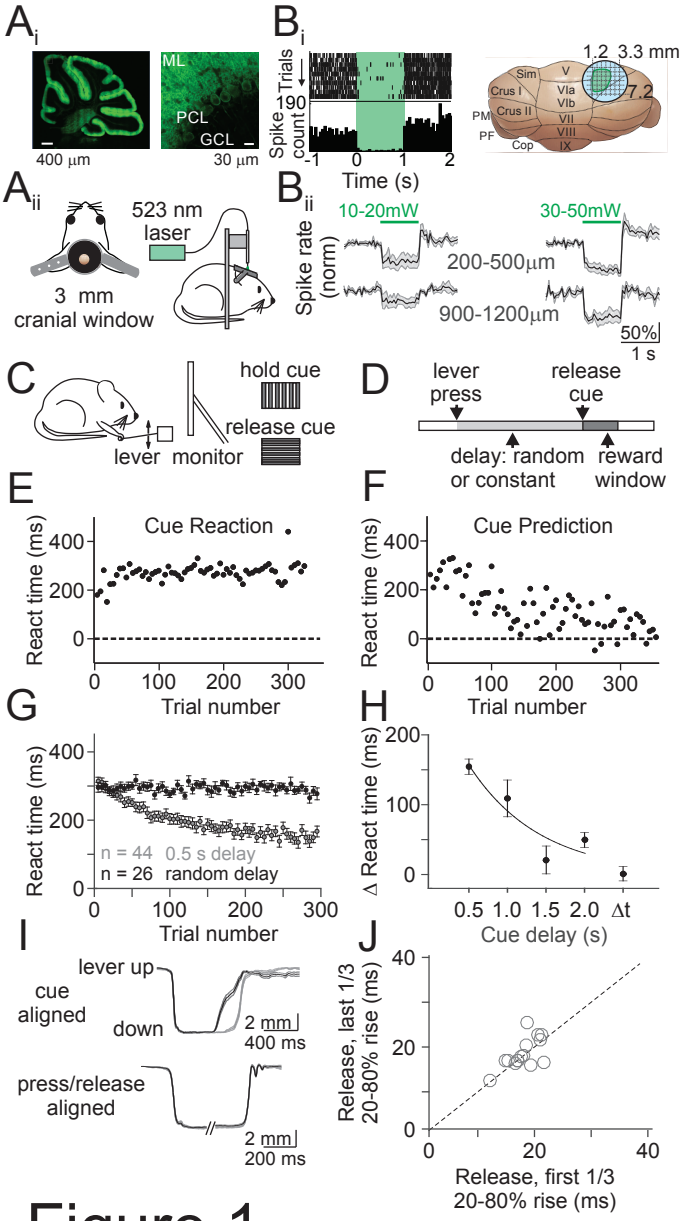
A_i
ML
PCL
GCL
400 µm
30 µm
B_i
Trials
190
Spike count
-1
0
1
2
Time (s)
1.2
3.3 mm
7.2
Sim
V
Crus I
VIa
VIb
Crus II
PM
VII
PF
VIII
Cop
IX
A_ii
523 nm laser
3 mm cranial window
B_ii
10-20mW
30-50mW
Spike rate (norm)
200-500µm
900-1200µm
50%
1 s
C
hold cue
release cue
lever
monitor
D
lever press
release cue
delay: random or constant
reward window
E
Cue Reaction
React time (ms)
400
200
0
0
100
200
300
Trial number
F
Cue Prediction
React time (ms)
400
200
0
0
100
200
300
Trial number
G
React time (ms)
400
200
0
n = 44 0.5 s delay
n = 26 random delay
0
100
200
300
Trial number
H
Δ React time (ms)
200
100
0
0.5
1.0
1.5
2.0
Δt
Cue delay (s)
I
lever up
cue aligned
down
2 mm
400 ms
press/release aligned
2 mm
200 ms
J
Release, last 1/3 20-80% rise (ms)
40
20
0
0
20
40
Release, first 1/3 20-80% rise (ms)

Figure 1

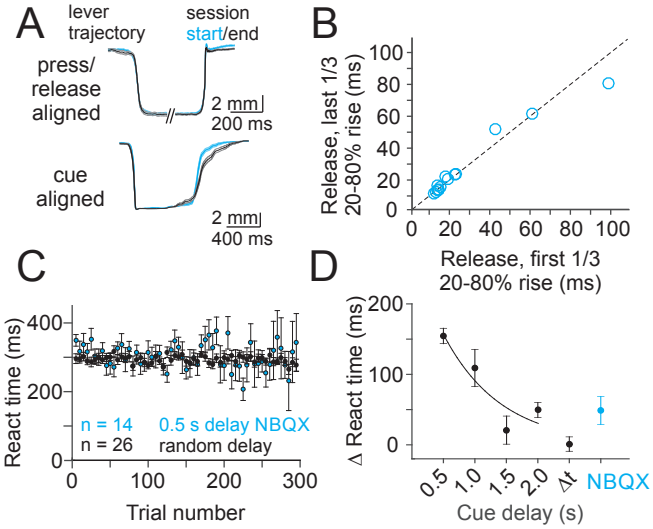
A
lever trajectory
session start/end
press/ release aligned
2 mm
200 ms
cue aligned
2 mm
400 ms
B
Release, last 1/3 20-80% rise (ms)
Release, first 1/3 20-80% rise (ms)
C
React time (ms)
n = 14
n = 26
0.5 s delay NBQX
random delay
Trial number
D
Δ React time (ms)
0.5
1.0
1.5
2.0
Δt
NBQX
Cue delay (s)

Figure 2

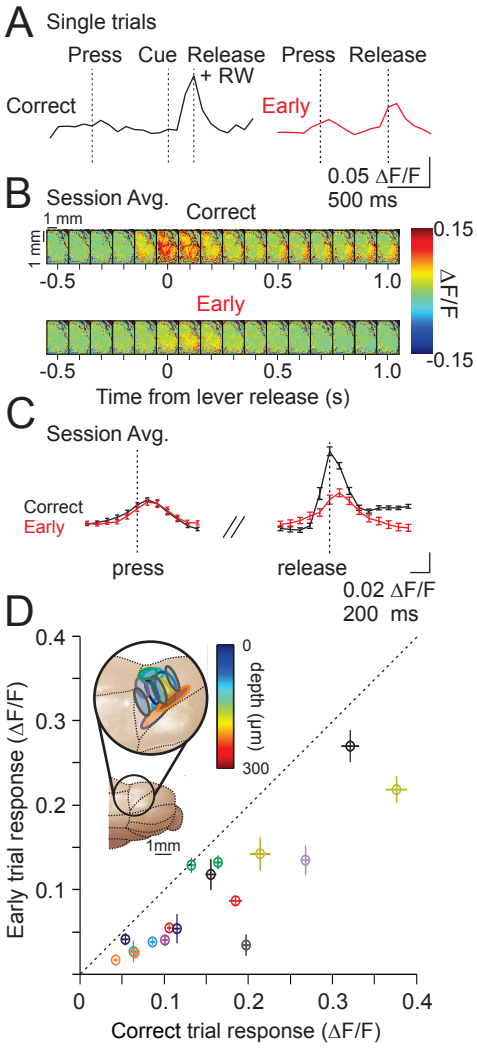
A
Single trials
Press
Cue
Release
+ RW
Press
Release
Correct
Early
0.05 ΔF/F
500 ms
B
Session Avg.
Correct
1 mm
1 mm
-0.5
0
0.5
1.0
Early
-0.5
0
0.5
1.0
0.15
ΔF/F
-0.15
Time from lever release (s)
C
Session Avg.
Correct
Early
press
release
0.02 ΔF/F
200 ms
D
0.4
0.3
0.2
0.1
Early trial response (ΔF/F)
0
0.1
0.2
0.3
0.4
Correct trial response (ΔF/F)
0
depth (μm)
300
1mm

Figure 3

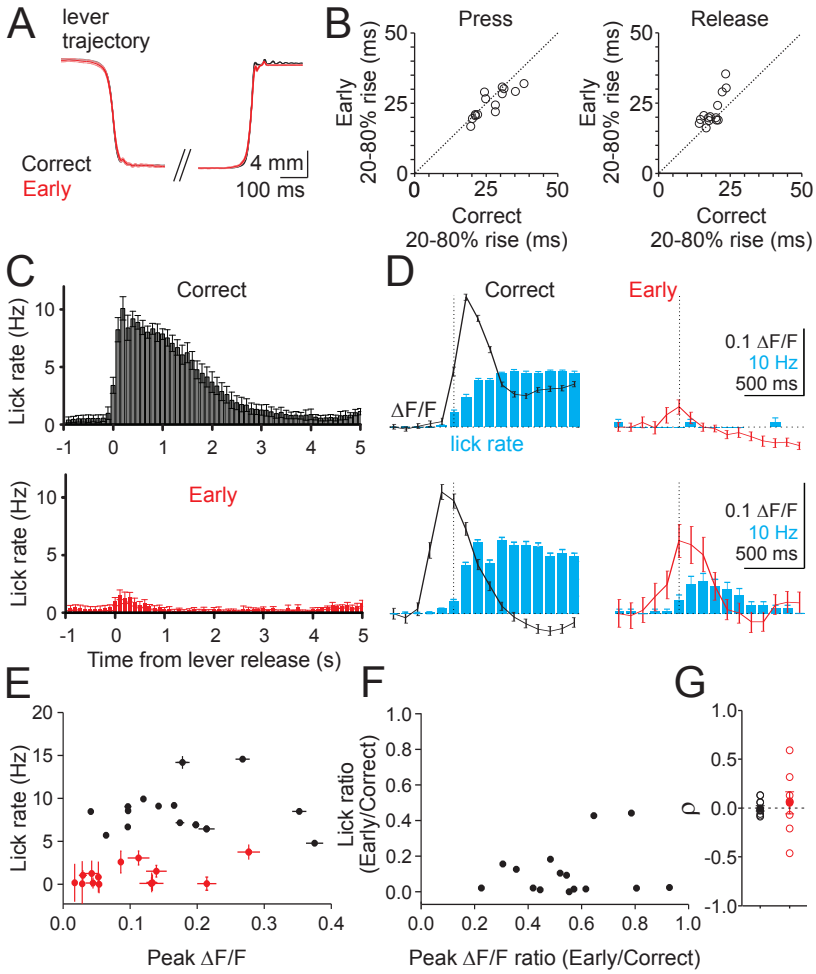
A
lever
trajectory
Correct
Early
4 mm
100 ms
B
Press
Release
Early
20-80% rise (ms)
Correct
20-80% rise (ms)
C
Correct
Early
Lick rate (Hz)
Time from lever release (s)
D
Correct
Early
ΔF/F
lick rate
0.1 ΔF/F
10 Hz
500 ms
E
Lick rate (Hz)
Peak ΔF/F
F
Lick ratio
(Early/Correct)
Peak ΔF/F ratio (Early/Correct)
G
ρ

Figure 4

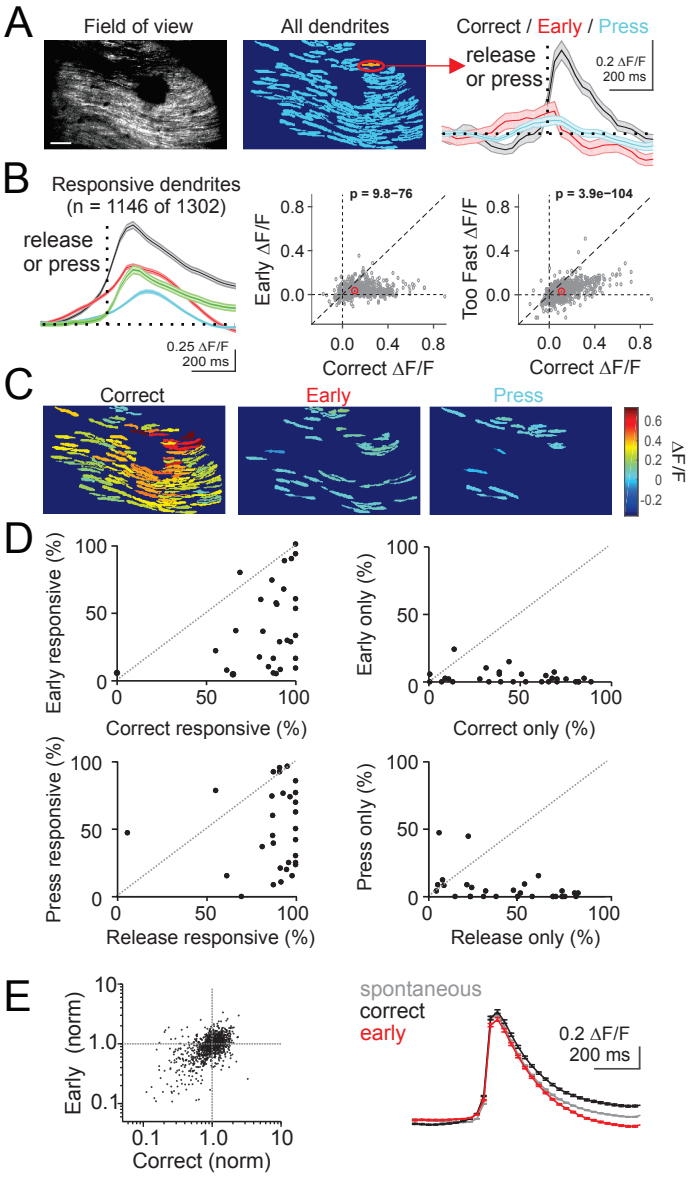
A
Field of view
All dendrites
Correct / Early / Press
release
or press
0.2 ΔF/F
200 ms
B
Responsive dendrites
(n = 1146 of 1302)
release
or press
0.25 ΔF/F
200 ms
p = 9.8−76
Early ΔF/F
Correct ΔF/F
p = 3.9e−104
Too Fast ΔF/F
Correct ΔF/F
C
Correct
Early
Press
ΔF/F
D
Early responsive (%)
Correct responsive (%)
Early only (%)
Correct only (%)
Press responsive (%)
Release responsive (%)
Press only (%)
Release only (%)
E
Early (norm)
Correct (norm)
spontaneous
correct
early
0.2 ΔF/F
200 ms

Figure 5

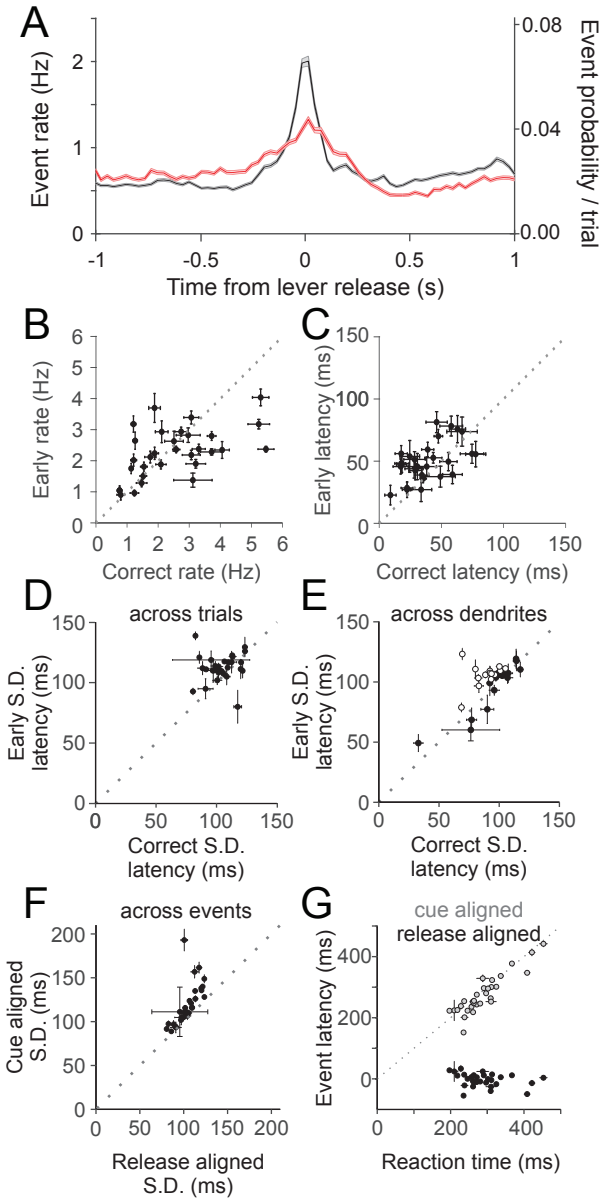
A
Event rate (Hz)
Event probability / trial
Time from lever release (s)
B
Early rate (Hz)
Correct rate (Hz)
C
Early latency (ms)
Correct latency (ms)
D
across trials
Early S.D. latency (ms)
Correct S.D. latency (ms)
E
across dendrites
Early S.D. latency (ms)
Correct S.D. latency (ms)
F
across events
Cue aligned S.D. (ms)
Release aligned S.D. (ms)
G
cue aligned
release aligned
Event latency (ms)
Reaction time (ms)

Figure 6

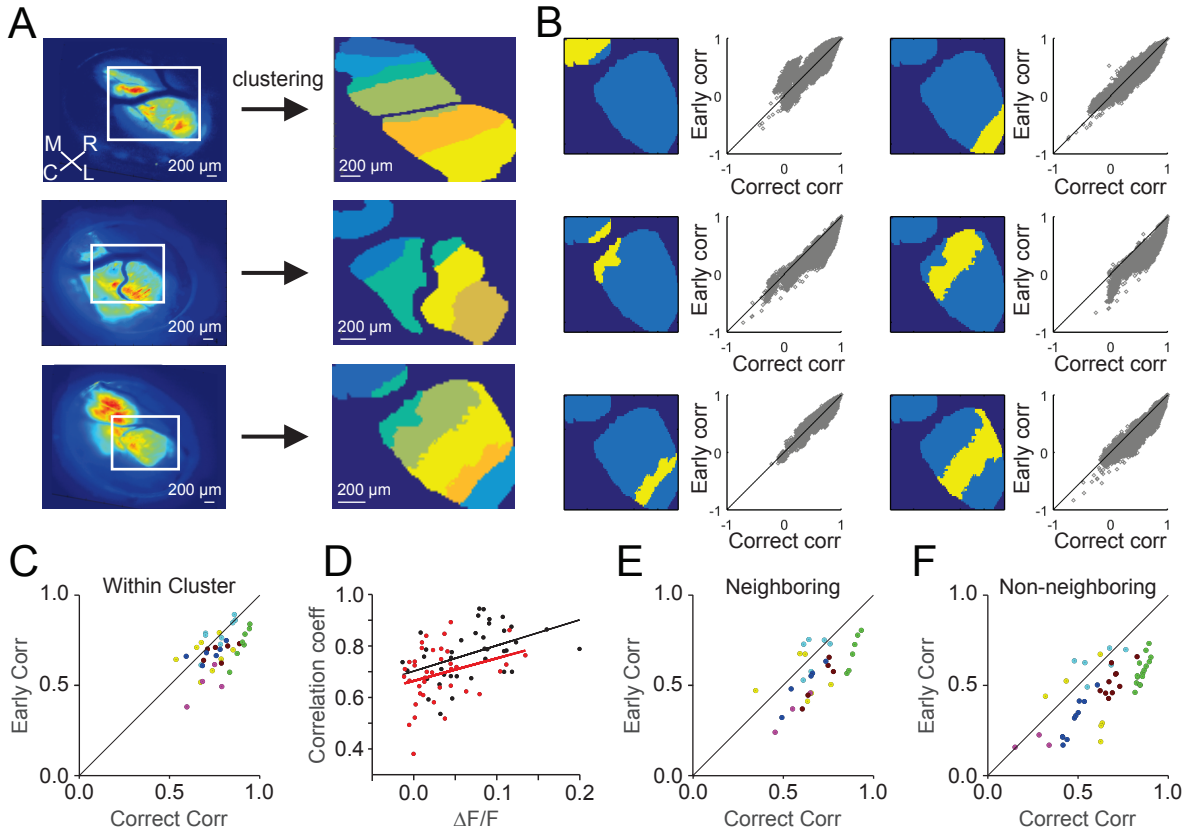
A
clustering
M
R
C
L
200 µm
B
Early corr
Correct corr
C
Within Cluster
Early Corr
Correct Corr
D
Correlation coeff
ΔF/F
E
Neighboring
F
Non-neighboring

Figure 7

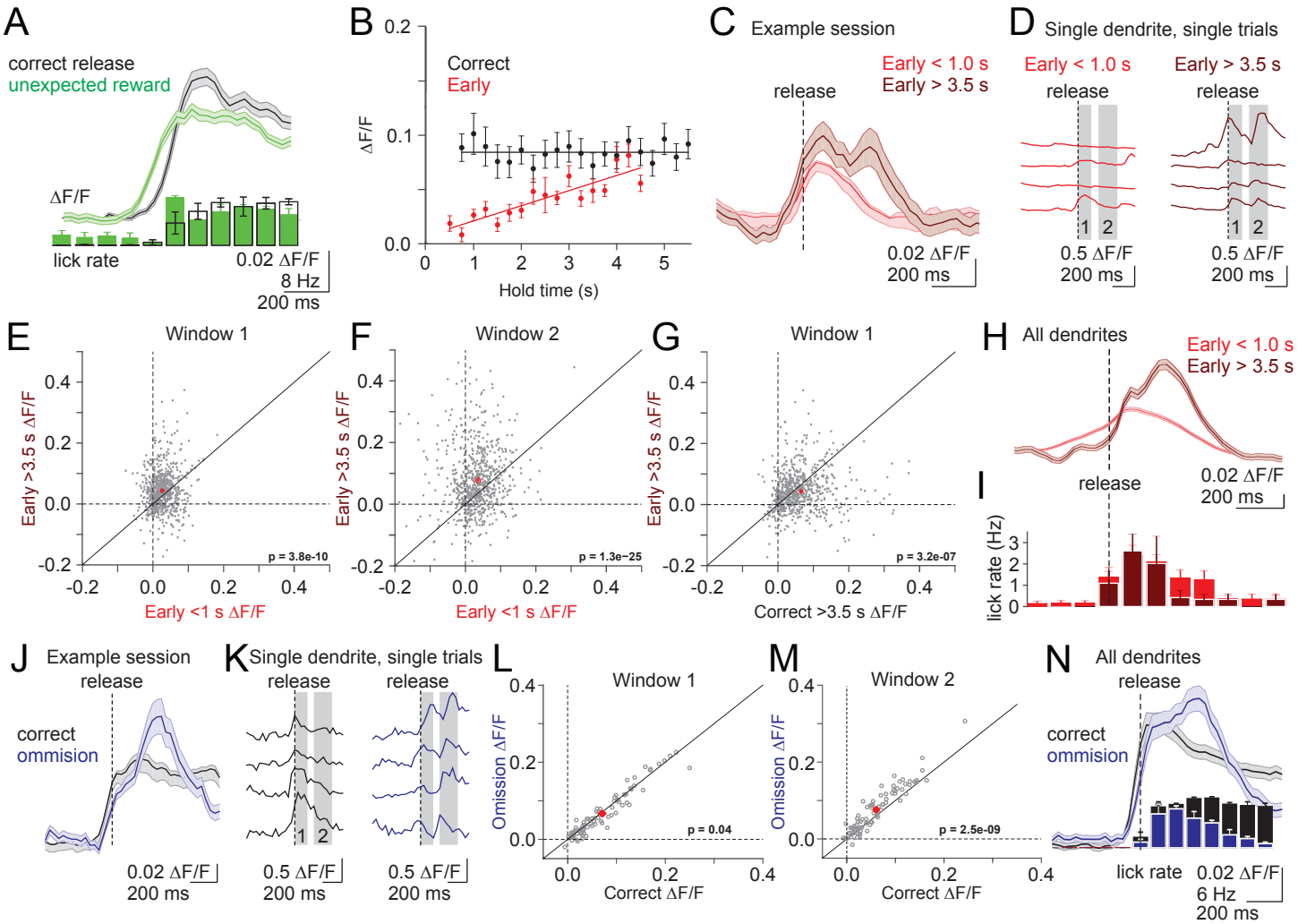
A
correct release
unexpected reward
ΔF/F
lick rate
0.02 ΔF/F
8 Hz
200 ms
B
Correct
Early
ΔF/F
Hold time (s)
C
Example session
release
Early < 1.0 s
Early > 3.5 s
0.02 ΔF/F
200 ms
D
Single dendrite, single trials
Early < 1.0 s
Early > 3.5 s
release
1
2
0.5 ΔF/F
200 ms
E
Window 1
Early >3.5 s ΔF/F
Early <1 s ΔF/F
p = 3.8e-10
F
Window 2
p = 1.3e−25
G
Window 1
Correct >3.5 s ΔF/F
p = 3.2e-07
H
All dendrites
Early < 1.0 s
Early > 3.5 s
release
0.02 ΔF/F
200 ms
I
lick rate (Hz)
J
Example session
release
correct
ommision
0.02 ΔF/F
200 ms
K
Single dendrite, single trials
release
0.5 ΔF/F
200 ms
L
Window 1
Omission ΔF/F
Correct ΔF/F
p = 0.04
M
Window 2
p = 2.5e-09
N
All dendrites
release
correct
ommision
lick rate
0.02 ΔF/F
6 Hz
200 ms

Figure 8

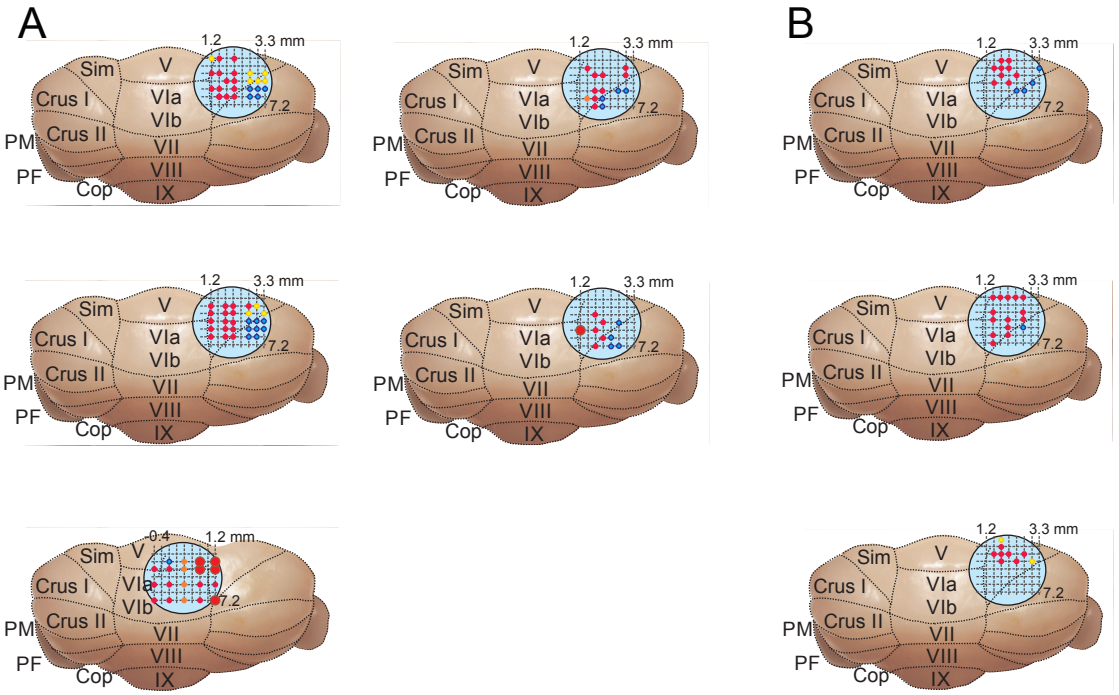

Arch: 5 mice
10-50mW, one Step pulse for 1sec

Right arm
Right & Left arms
Very weak arm movements
Whiskers or mouth or nose
nothing

Electrical Stim. 3 mice
0.1mA-1mA
50Hz for 500ms or 1sec

Right arm
Right & Left arms
Very weak arm movements
Whiskers or mouth or nose
nothing

supplemental figure 1

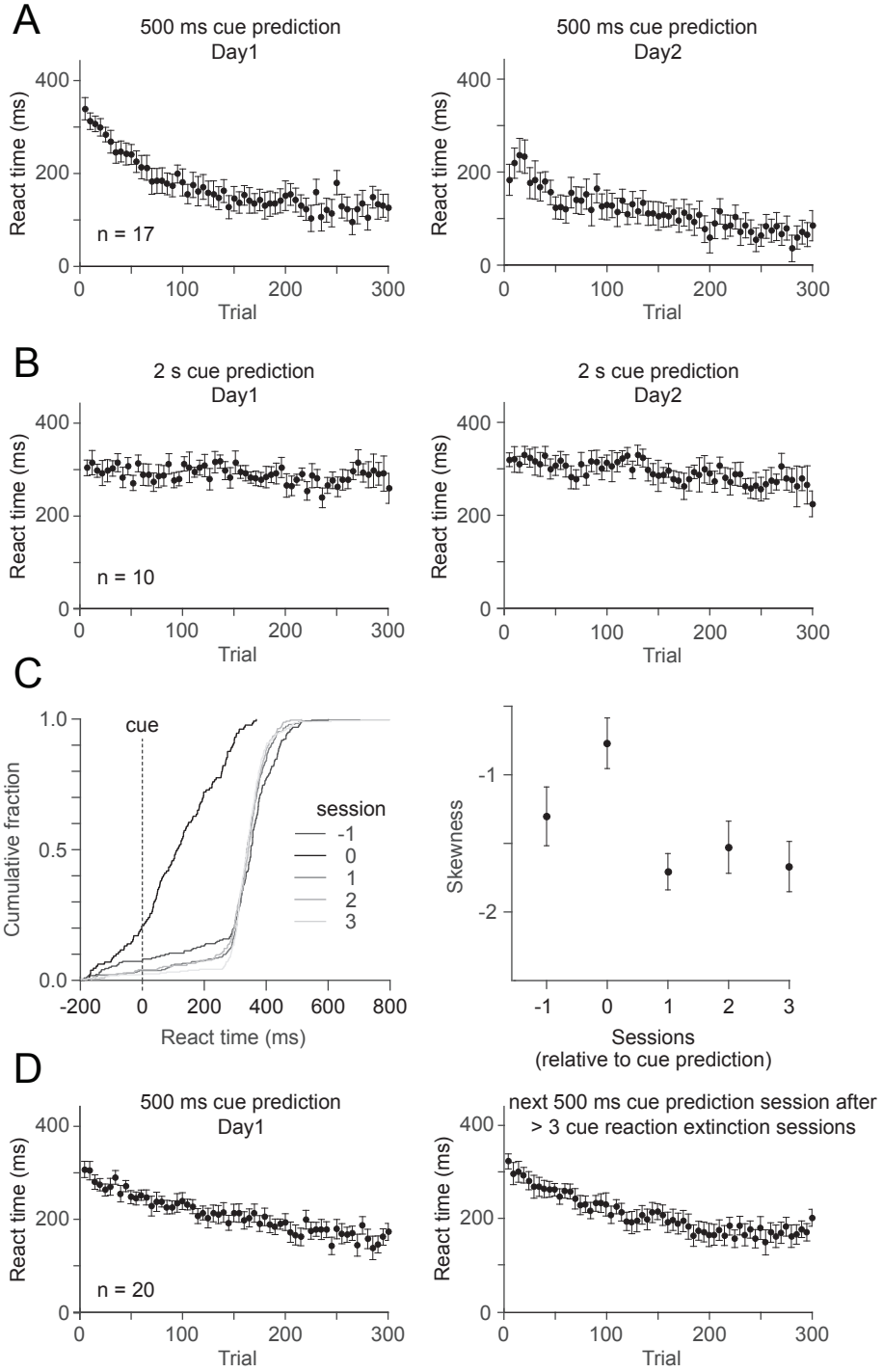

supplemental figure 2

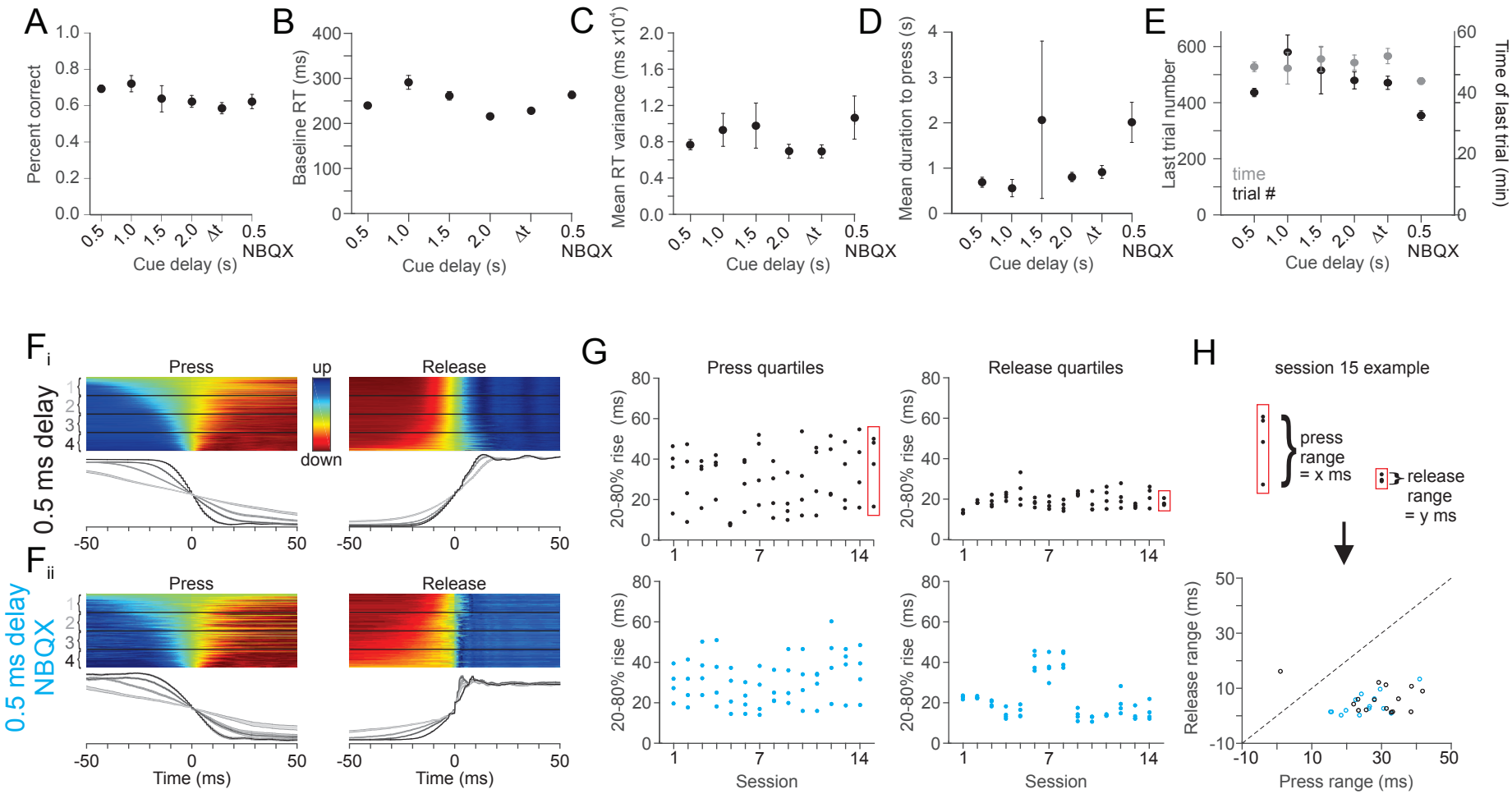

supplemental figure 3

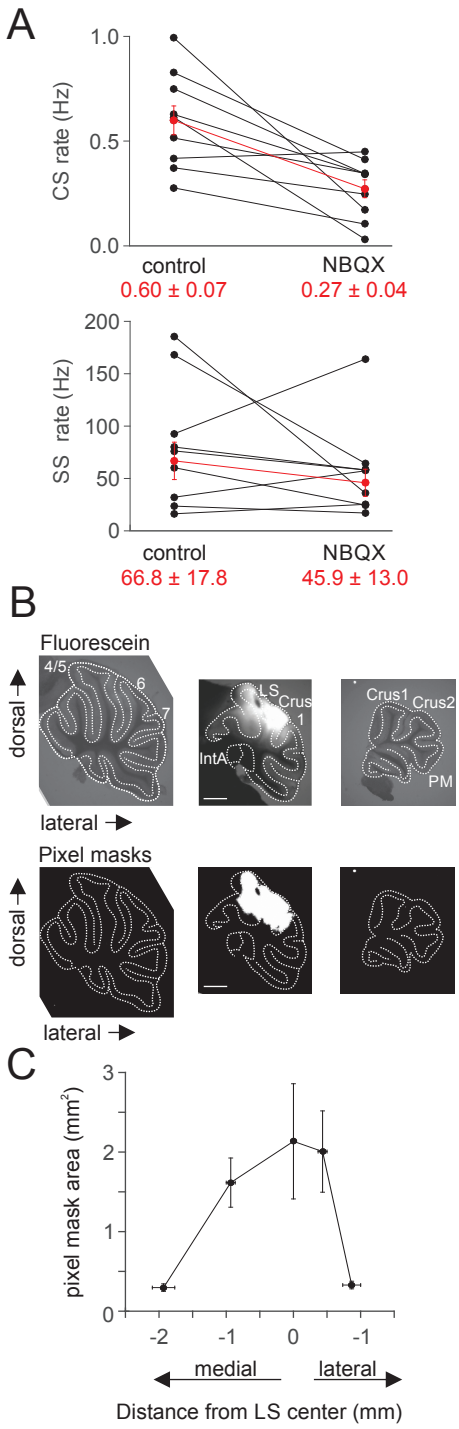

supplemental figure 4

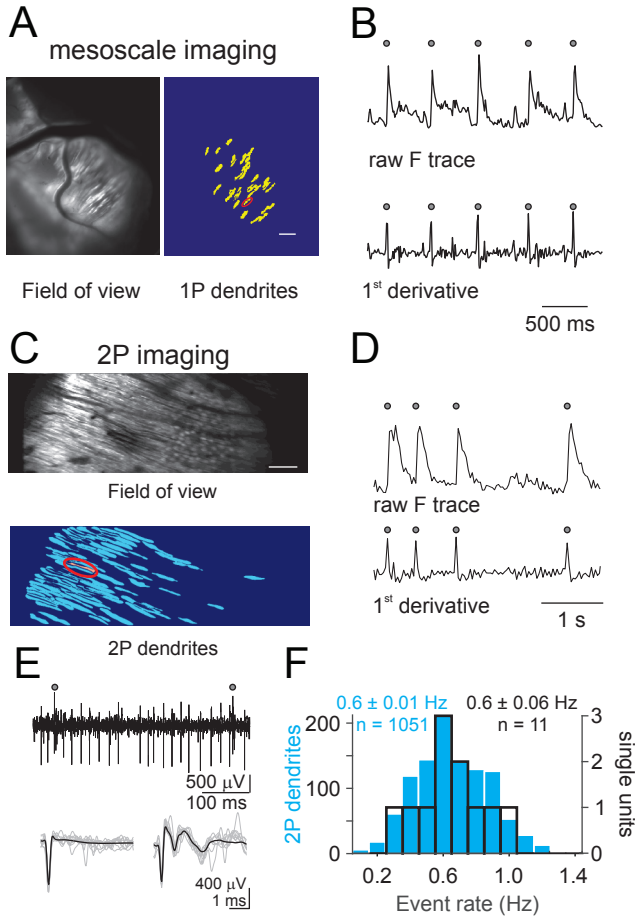

supplemental figure 5

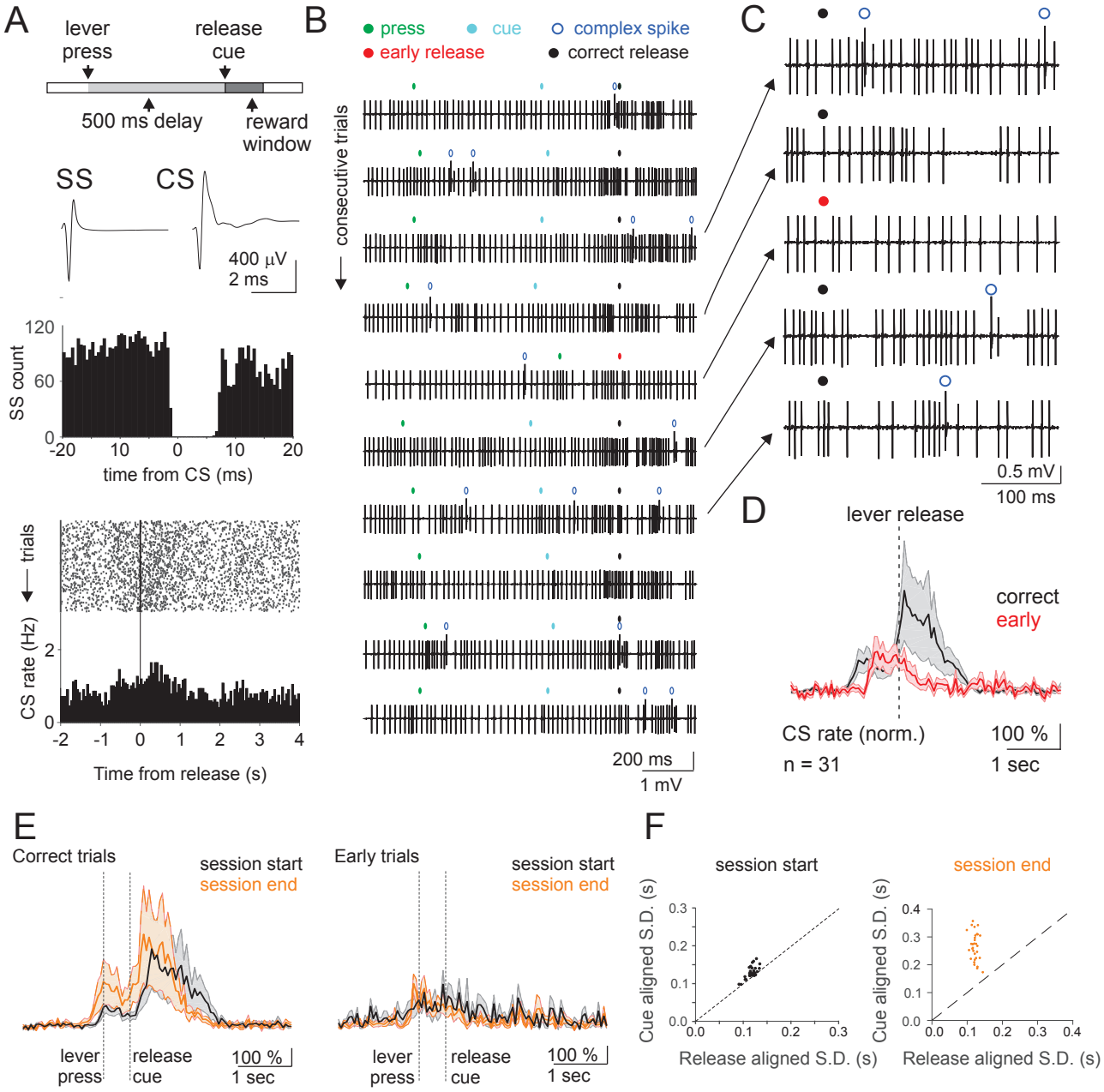

mean release aligned S.D. = 0.118 ± 0.002
mean cue aligned S.D. = 0.130 ± 0.003
p =3.7e-06

mean release aligned S.D = 0.123 ± 0.002
mean cue aligned S.D. = 0.265 ± 0.009
p = 1.7e-15

supplemental figure 6

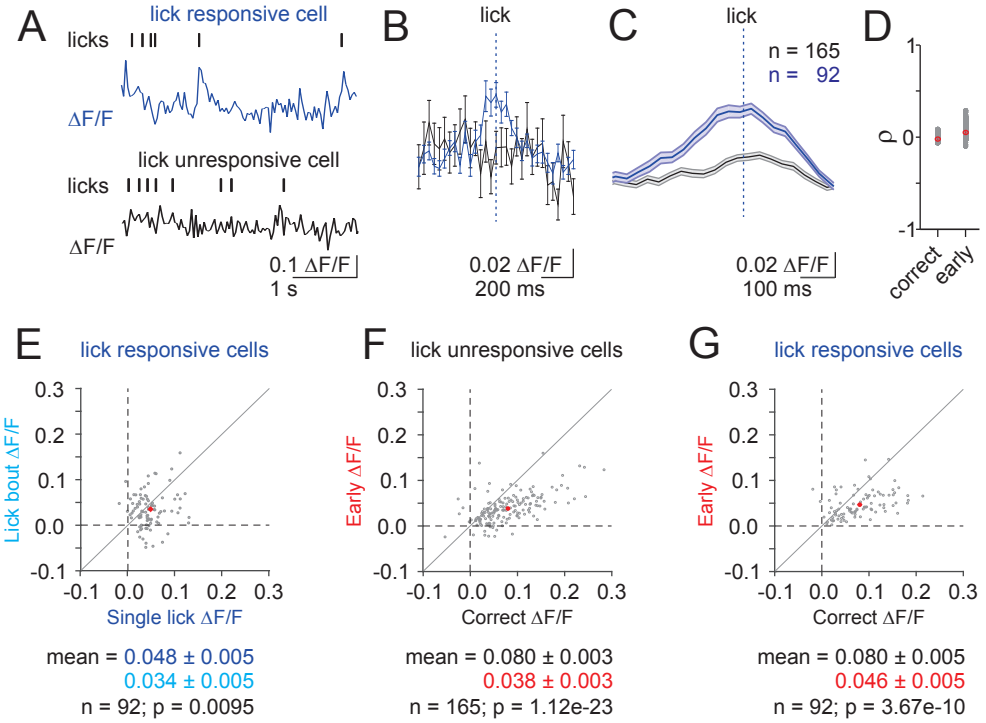

supplemental figure 7

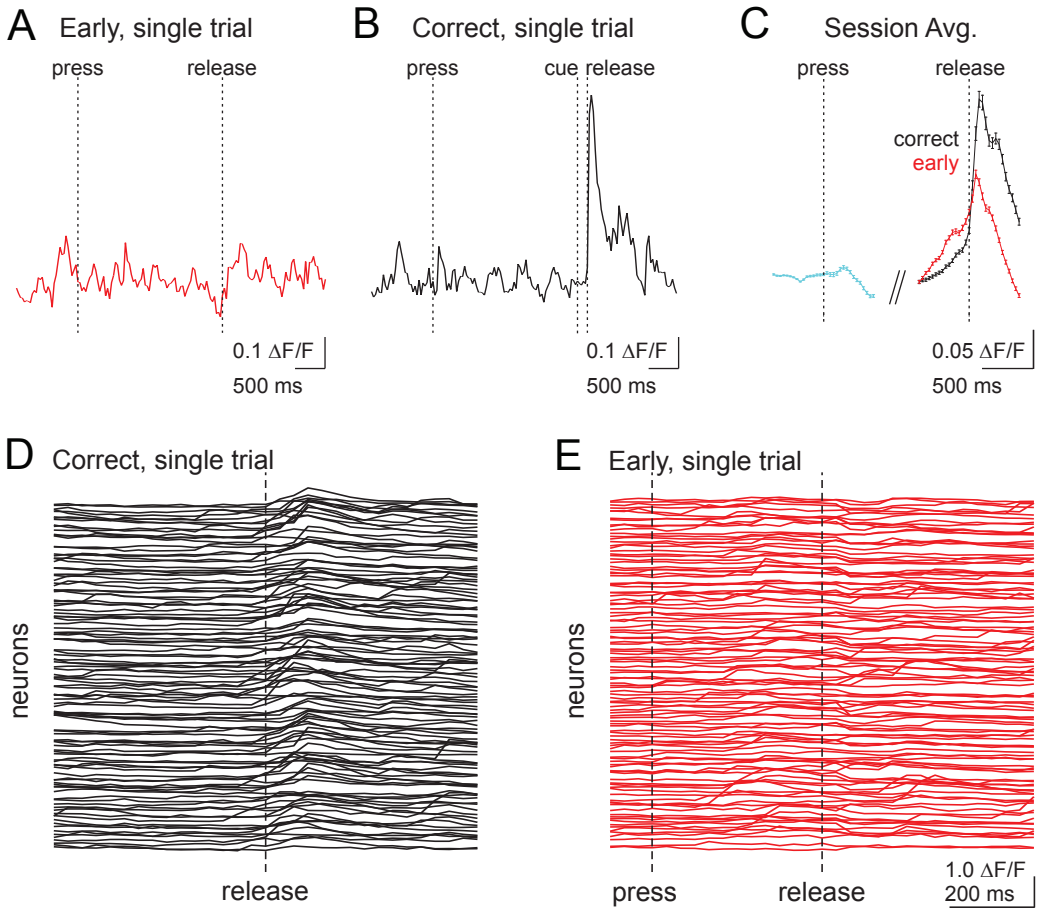

supplemental figure 8

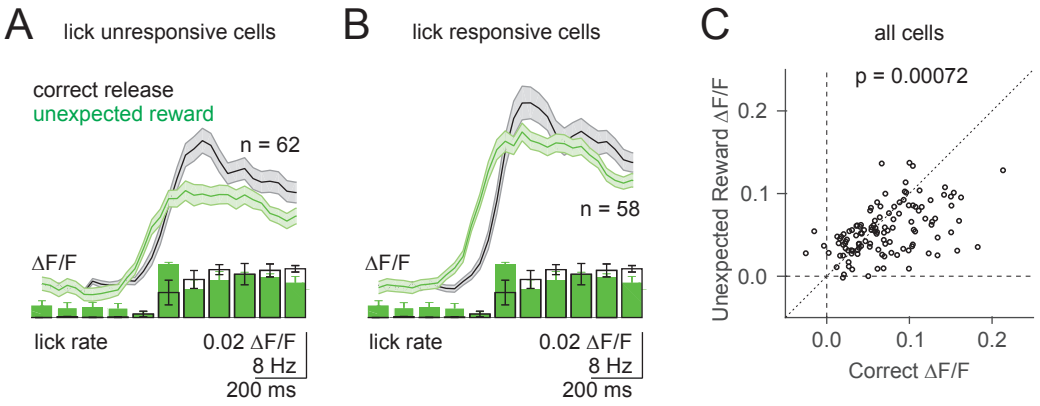

supplemental figure 9

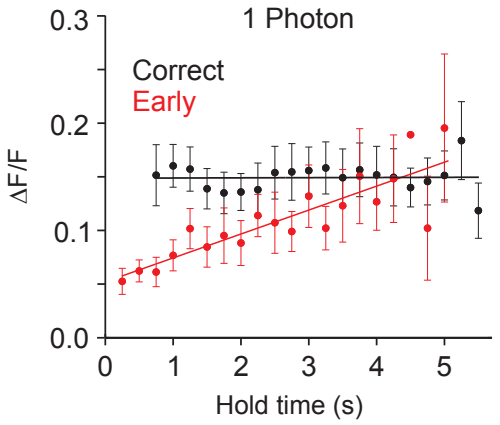

supplemental figure 10

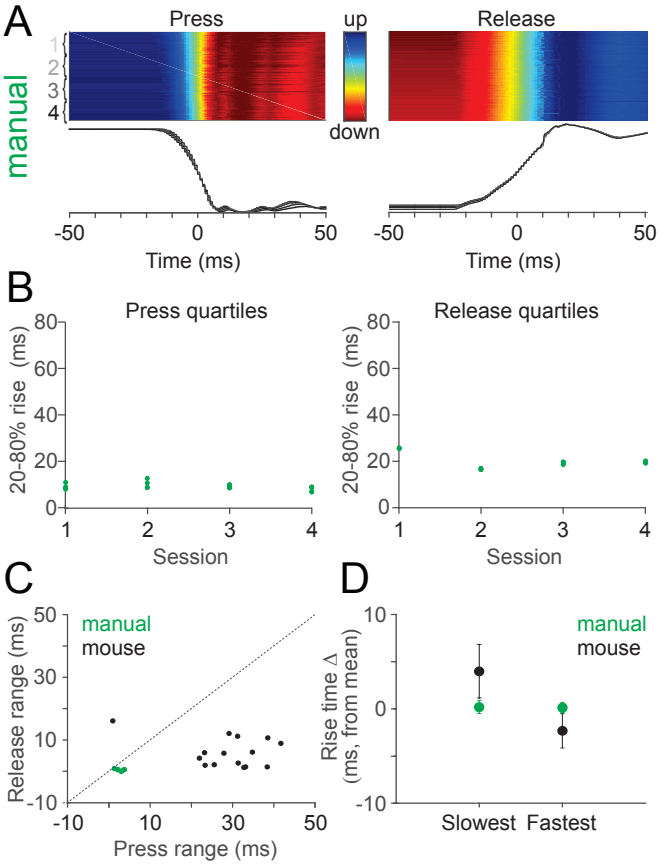

supplemental figure 11